Journal of Energy Storage 86 (2024) 111230

Contents lists available at ScienceDirect

Journal of Energy Storage

journal homepage: www.elsevier.com/locate/est

Research papers

Predictive power fluctuation mitigation in grid-connected PV systems with rapid response to EV charging stations

Darío Benavides [a,b], Paul Arévalo [b], Edisson Villa-Ávila [b,c], José A. Aguado [a], Francisco Jurado [b,*]

[a] Department of Electrical Engineering, University of Málaga, 29010 Málaga, Spain
[b] Department of Electrical Engineering, University of Jaén, 23700 Jaén, Spain
[c] Department of Electrical, Electronics and Telecommunications Engineering, University of Cuenca, 010107 Cuenca, Ecuador

ARTICLE INFO

Keywords:
Power fluctuations
Renewable energy systems
Photovoltaic technology
Electric vehicle demand
Power smoothing

ABSTRACT

Currently, renewable energies and electric vehicle charging stations are essential for energy sustainability. However, the variable generation from renewable sources, such as photovoltaic systems, can lead to power peaks that impact the stability of the grid. This challenge is exacerbated by the increasing demand in fast-charging stations. Addressing these demand peaks is crucial to ensure the stability of the electrical grid. This paper introduces the predictive-flex smoother, an innovative method designed to mitigate power fluctuations in grid-connected photovoltaic systems while optimizing energy management in electric vehicle charging stations. The predictive-flex smoother method incorporates a hybrid energy storage system comprising supercapacitors and vanadium redox flow batteries to respond rapidly to electric vehicle charging stations demands, enhance grid electricity purchase optimization, and improve energy quality delivery. The proposed method integrates two control strategies: photovoltaic fluctuation reduction strategy and peak demand reduction strategy for electric vehicle charging stations. By leveraging prediction algorithms and machine learning techniques, the predictive-flex smoother method achieves precise power fluctuation forecasts, allowing efficient utilization of supercapacitors and vanadium redox flow batteries to smooth photovoltaic power fluctuations and reduce electrical vehicles peak demand. Comprehensive experimental investigations and simulations validate the method's performance under various operational conditions. The results demonstrate the effectiveness of the predictive-flex smoother method, significantly improving the quality of power delivered to the grid while reducing costs. The experimental platform, validates the real-time response of the proposed method, with response times under 500 ms. The experimental results further confirm the efficiency of the method in power smoothing and charging strategies with varying electrical vehicles models and connection coefficients.

Symbology

P_{SC}	Supercapacitor power
C_{SC}	Cost of SC
C_{PV}	Cost of PV
N_{EV}	Number of EVs
C_{VR}	Cost of VRFB
Δt_{EV}	Charging time of EV
t	Time
Δt^{SC}	SC time interval
$P^{SC}{}_{ref}$	Reference power value for the SC
$P^{VR}{}_{ref}$	Reference power value for the VRFB
Δt^{VR}	VRFB time interval
t (t)	Index for time periods
X_t	Output power of the PV installation (without smoothing) at instant t
$X_{t-NMA^{SC}+t-1}$	Predicted PV values for a very short time interval for SC

(continued on next column)

(continued)

(continued on next page)

Abbreviations: PFS, Predictive-flex smoother; PV, Photovoltaic; SC, Supercapacitor; ESS, Energy storage systems; BESS, Battery energy storage system; HESS, Hybrid energy storage system; EVCS, Electric vehicle charging station; EV, Electric vehicle; TEV, Electric taxi; MA, Moving average; RR, Ramp rate; PCC, Point common connection; SOC, State of charge; VRFB, Vanadium redox flow batteries; PFS, Predictive-flex-smoother method; RES, Renewable energy sources; G2V, Grid-to-vehicle; V2G, Vehicle-to-grid; PSCAD, Power systems computer aided design; CCTI-B, Micro-grid laboratory at the University of Cuenca; SCADA, Supervisory control and data acquisition; AC, Alternating current.

* Corresponding author.
E-mail address: fjurado@ujaen.es (F. Jurado).

https://doi.org/10.1016/j.est.2024.111230
Received 21 September 2023; Received in revised form 4 March 2024; Accepted 5 March 2024
Available online 13 March 2024

(*continued*)

$X_{t-NMA^{VR}+t-1}$	Predicted PV values for a very short time interval for VRFB
η_C^{SC}	SC performance during the storage charge process
η_D^{SC}	SC performance during the storage discharge process
η_C^{VR}	VRFB performance during the storage charge process
η_D^{VR}	VRFB performance during the storage discharge process
CC	SC reference power correction intensity modulation coefficient
R_{max}^{SC}	SC maximum ramp value control
R_{max}^{VR}	VRFB maximum ramp value control
SOC_{min}^{SC}	SC minimum state of charge
SOC_{max}^{SC}	SC maximum state of charge
SOC_{min}^{VR}	VRFB minimum state of charge
SOC_{max}^{VR}	VRFB maximum state of charge
P	Nominal power of the renewable PV system
NMA^{SC}	Number of periods used to calculate the SC moving average
NMS^{SC}	Number of periods used to calculate the variation in the energy contained in the SC storage
NMA^{VR}	Number of periods used to calculate the VRFB moving average
NMS^{VR}	Number of periods used to calculate the variation in the energy contained in the VRFB storage
vs_t^{SC}	Power transferred from the PV panels to SC storage in period t (cut peaks)
$vs^{SC}{}_{t-NMS^{SC}+t-1}$	Power transferred from SC storage to the grid in very short time interval
sr_t^{SC}	Power transferred from SC storage to the grid in period t (fill gaps)
$sr^{SC}{}_{t-NMS^{SC}+t-1}$	Power transferred from the PV panels to SC storage in very short time interval
SOC_t^{SC}	Energy contained in SC storage at the end of period t
vs_t^{VR}	Power transferred from the PV panels to VRFB storage in period t (cut peaks)
$vs^{VR}{}_{t-NMS^{VR}+t-1}$	Power transferred from VRFB storage to the grid in very short time interval
sr_t^{VR}	Power transferred from VRFB storage to the grid in period t (fill gaps)
$sr^{VR}{}_{t-NMS^{VR}+t-1}$	Power transferred from the PV panels to VRFB storage in very short time interval
SOC_t^{VR}	Energy contained in VRFB storage at the end of period t
$\widehat{p_t}^{SC}$	SC reference power prediction value using the moving average method
$\widehat{p_t}^{VR}$	VRFB reference power prediction value using the moving average method
$\Delta soc_t{}^{SC}$	Value of the average variation of power in SC storage
$\Delta soc_t{}^{VR}$	Value of the average variation of power in VRFB storage
P_{EV}	Power of EV charging
SOC_{EV}	EV battery state of charge
SY	Average annual mileage of an EV
T_{EV}	Number of days an electric vehicle drives per year
SD	Range of EV battery
X_{EV}	Electric demand for charging power of EVs
M_{EV}	EV connection coefficient, which is between 0 and 1
λ_{EV}	Current forecast number of EVs
γ_{EV}	EV charging time per day
p_t	PV power value obtained in real time
$p_t(t+1)$	PV power value obtained in the subsequent time step
P_{GPV}	Peak PV power considers for full EV charge
$f_{pv}(t)$	PV power fluctuation calculated at two-time instants
$\frac{dp_t(t)}{dt}$	Change rate of power value obtained in real time
Δt	Time interval.
Pn	Nominal PV power
CC	Modulation coefficient
p_t	Instant renewable power
$f_{pv}(n)$	$d-$ dimensional vectors
Sf_{pv}	Elements are the PV fluctuations $f_{pv}(j)$ represented by data vectors
$E(\mu_i)$	The objective function representing the sum of squared distances of each fluctuation group from its cluster centroid
k	The total number of clusters or centroids
μ_i	Centroid of k-means algorithm
F_T	Cumulative EV consumption until time T
m	Maximum coefficient of sales on the market
p	Innovation coefficient
q	Imitation coefficient
P_{GRID}	Power from the grid
P_{PFS}	Output power of the FPS method
$k_{\#positive}$	Number of positive fluctuations
$k_{\#negative}$	Number of negative fluctuations

1. Introduction

1.1. Context and motivation

Environmental concerns, technological advancements, and cost reductions are driving the expansion of renewable energy sources (RES) and electric transportation [1]. Among various RES photovoltaic (PV) technology has experienced significant growth, playing a crucial role in achieving a sustainable future [2]. However, the intermittent nature of PV and sporadic electric vehicle (EV) demands pose challenges to power supply stability and reliability [3]. These power fluctuations affect energy delivery, calling for power smoothing methodologies to enhance grid or localized system quality and reliability [4]. Integrating energy storage systems (ESS), electric vehicle charging stations (EVCS), and PV systems offers a promising solution for power smoothing [5]. Supercapacitors (SC) have garnered attention due to their high-power density and responsiveness, effectively attenuating fluctuations in RES [6]. Recent studies confirm the effectiveness of SCs in mitigating load peaks and ensuring stable energy output [7,8].

Flow batteries, such as vanadium redox flow batteries (VRFB), are another attractive option due to their energy density and prolonged storage capacity. They allow flexible energy management by gradually releasing stored energy to address fluctuations [9]. Moreover, these batteries are non-degradable over time, providing an almost unlimited number of charge and discharge cycles without efficiency loss, unlike lead-acid or lithium batteries. In PV systems supplying grid-connected EVs, ensuring energy quality and reliability requires optimizing the ESS's operability. This paper focuses on PV systems with hybrid storage (SC + VRFB) that supply EVs through EVCSs.

1.2. Literature review

The literature review reflects a growing interest in developing efficient and reliable solutions to address power fluctuations in RES. These methods have gained significant attention due to the challenges posed by intermittent generation and the variability of RES. A notable contribution, as outlined in [10], the authors introduce a multipurpose control mechanism that not only prevents reverse power flow but also optimally manages the state of charge (SOC) of batteries through a sophisticated energy smoothing system at the substation level. Simulation studies support the efficacy of this mechanism in achieving precise control objectives, identifying optimal locations for battery energy storage systems (BESS), and determining suitable types of BESS. Further enriching the literature, [11] explores an exponential linear smoothing technique for power smoothing, guided by a reference signal. The potential for refinement through predicting power fluctuations with higher precision is emphasized. Advanced algorithms and operation strategies, as discussed in [12], leveraging real-time data on power generation, load demand, and relevant parameters. Research on a hybrid energy storage system (HESS) composed of SCs and BESS, as presented in [13], introduces an optimization feedback control mechanism fortified by dual Kalman filters and a robust predictive control model. This intricate control paradigm not only enhances BESS longevity but also effectively mitigates power variations, thereby alleviating strain on SCs. Despite these advances, there is a limited analysis of the cost implications associated with energy storage devices, especially energy smoothing storage systems [14]. This study addresses this gap by proposing an innovative approach that leverages EV demand prediction to effectively smooth PV power and EV demand, avoiding the need for excessively large-scale traditional battery swapping stations.

As we transition from the literature review to a comprehensive exploration of possible application fields, it is essential to note the various methods researchers have employed for power smoothing using SCs and BESSs. The authors in [15] provide a solution to the intermittent and stochastic nature of renewable energy management using HESS to maximize energy production and ensure service continuity.

Additionally, [16,17] introduce approaches to mitigate the impact of EV charging, such as smart charging or grid-to-vehicle (G2V) and vehicle-to-grid (V2G). Effective energy control, as discussed in [18], can harness the significant storage resources provided by EVs, influencing future electrical grid operation and expansion plans. However, challenges persist in providing demand response through V2G and G2V, primarily due to uncertainties regarding EV availability and the potential impact of V2G system aging on expensive EV batteries. While some studies introduce energy allocation methods considering power fluctuations of PV and BESS [19], there is a risk of overlooking future power peaks, leading to oversized BESSs and increased system costs. In [20], a fuzzy logic-based control system is presented to level daily load based on V2G capacity, relying primarily on the current battery SOC. Steady-state applications utilizing EV capacities, such as load management and power smoothing, have been extensively explored in the literature [21–23]. However, few studies propose EV demand prediction systems to proactively reduce the power peaks they generate, and there is a notable lack of research on predicting applications of VRFB for EVs [24]. VRFBs have been evaluated for energy storage and fast EV charging. Important advantages are highlighted such as large storage capacity, greater design flexibility, nearly unlimited lifespan, and the ability to reuse deactivated underground gas tanks for installation at service stations, supporting the transition to electric mobility.

To further enrich the literature review, several studies have investigated the collective impact of individual RES on power smoothing. A study in [25] emphasizes the implementation of grid-connected ESS with SOC control for PV systems, demonstrating the efficacy of power smoothing methodologies in attenuating RES variability. Mathematical verification and case studies with power systems computer aided design (PSCAD) software simulations support the logical proof of methodology effectiveness. Similarly, [26] focuses on evaluating power smoothing techniques for PV output, introducing a comprehensive methodology for systematic evaluation. This study not only compares the performance of different power smoothing methods but also considers their impact on the BESS lifetime. The findings highlight the effectiveness of Fourier analysis-based power smoothing methods and emphasize the crucial role of SOC in influencing battery capacity loss. In the context of grid-integrated PV systems, [27] proposes an adaptive smoothing framework to address power fluctuations caused by passing clouds. The study introduces a predictive and adaptive controller with two layers, effectively reducing stress on the ESS by dynamically adjusting filter time constants based on real-time power RR. The results demonstrate improved power smoothing and reduced battery degradation compared to fixed time constant-based techniques. Furthermore, [28] investigates the stability and power-smoothing performance of a HESS integrated with a large-scale hybrid wind and PV farm. The proposed HESS, consisting of a VRFB and a SC, effectively enhances system stability and mitigates power fluctuations. The study employs steady-state and transient simulations to validate the positive impact of the HESS on power smoothing.

Considering the impact of RES on the reliability of PV inverters in active distribution grids, [29] introduces a PV inverter reliability-constrained control method. This approach incorporates power smoothing to ensure efficient power loss minimization while addressing uncertainties in PV generation and loads. The study employs a penalty convex-concave programming method, demonstrating the high efficiency of the proposed method in both minimizing power losses and enhancing PV inverter reliability. In the realm of wear-out analysis, [30] explores the implications of BESS converters performing peak shaving and harmonic current compensation operations. The study reveals a trade-off, with harmonic current compensation operations enhancing grid power quality but affecting the reliability of the BESS converter. The findings underscore the need for careful consideration of the balance between enhanced power quality and BESS reliability. Lastly, [31] introduces a HESS employing a VRFB and SC for grid-integrated PV systems. The proposed control strategy, incorporating a mixed-order generalized integrator and improved sparrow search algorithm tuned tilt integral–derivative with filter controller, effectively manages power fluctuations. The study demonstrates the overall effectiveness of the proposed control strategy under various conditions, highlighting its potential for high-energy and power support.

The authors in [32] present an innovative power smoothing technique using fuzzy logic in electric vehicle batteries to optimize self-consumption and reduce power fluctuations for island power systems. The behavior of the battery energy storage system of EVs has also been studied as a control strategy to smooth out the fluctuations of wind energy composed of several EVAs with different response parameters [33]. This study highlights the adaptive SOC method and the energy production limits restricted by maximum operating areas. Recent studies also propose multi-agent deep reinforcement learning for fast charging stations for electric vehicles, which smoothes the spatial distribution of electric vehicle charging demands and reduces traffic congestion in the electrical grid [34].

The reviewed research provides practical applications in the field of renewable energies and energy fluctuation control. The multipurpose approach of [10] presents applications in efficient battery management and the mitigation of challenges associated with intermittent generation. The exponential linear smoothing technique of [11] emphasizes the improvement in the accuracy of predicting energy fluctuations. Advanced algorithms and real-time operational strategies, as described in [12], are applicable to energy smoothing in PV systems, explored in [13]. The prediction of EV demand to smooth solar energy generation, proposed in [14], offers a practical application for optimizing EV charging infrastructure. These applications illustrate the possibilities derived from the literature review in the field of renewable energies and energy storage.

1.3. Research gaps

In the literature review, a growing interest has been observed in the development of efficient and reliable solutions to address power fluctuations in RES. However, there are still some research gaps. The main identified gaps are as follows:

- Although BESS have been proposed to reduce power fluctuations in PV and EVCS, the disadvantages related to their lifespan and replacement costs due to deep charge/discharge cycles have been overlooked [10,11].
- Despite the usefulness of SCs in mitigating fluctuations in RES, their potential has been underestimated by not fully analyzing the advantages of combining them with BESS using fluctuation prediction algorithms [12]. In a previous work by the authors in [12], the feasibility of the fluctuation prediction method was demonstrated, but BESS and EVCS were not considered. In addition, for this study, a controller is implemented that integrates the hybrid SC and VRFB systems, enabling a reduction in the ramp rate to approximately 1 %. This demonstrates robust response and establishes a strategy for optimal peak reduction in EVCS. Similarly, the controller integrates the proposed vehicle charging power prediction from [35], utilizing hybrid storage systems to mitigate peaks in EVCS.
- HESS combining SCs, and BESS have been examined, but most studies have focused on lead-acid and lithium-ion batteries, neglecting promising technologies like VRFB in conjunction with SCs [19].
- It is necessary to optimize the operability of HESS through long-term fluctuation predictions, as the stochastic nature of PV energy requires longer intervals to obtain accurate values [12,24].
- Energy management in V2G or G2V systems must consider the impact of PV power peaks matching with multiple EVCS charging or discharging power peaks to improve grid stability and leverage the benefits of fluctuation prediction through the combination of RR and MA methods [13,17,20].

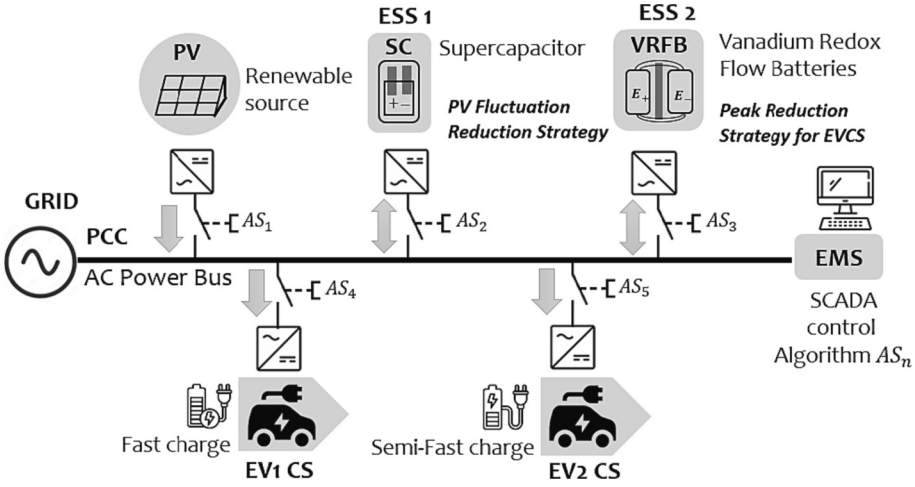

Fig. 1. Design and architecture of the proposed hybrid renewable system.

- The proposed adaptive smoothing framework for grid-integrated PV systems, as presented in [27], introduces a predictive and adaptive controller to address power fluctuations. However, further investigation is needed to explore the broader applicability of this framework and potential refinements for diverse weather conditions.
- The HESS proposed in [31] combining a VRFB and SC shows promise in managing power fluctuations. However, research gaps persist in assessing the economic viability, scalability, and potential integration challenges of this specific HESS configuration in grid-integrated PV systems.

1.4. Contributions and paper organization

To address the previously identified research gaps, this paper introduces an innovative method called "predictive-flex smoother" (PFS). Its objective is to mitigate energy fluctuations in PV systems connected to the grid by using a HESS that combines SC and VRFB. This approach enables a rapid response to the demand of EVCS, optimizing electricity purchase from the grid and improving the energy quality delivered to it.

The joint control system relies on two innovative strategies: the first aims to reduce PV fluctuations, while the second targets peak demand reduction for EVCS. To achieve this, prediction is employed to calculate the EV charging energy demand, minimizing the impact on the grid through VRFB storage and achieving zero consumption from the electric grid. The method's effectiveness and performance were evaluated through experimental research and simulations under various operational situations and conditions.

The main scientific contributions of this approach lie in the combination of RR and MA methods with machine learning techniques to prediction mechanism for PV-induced power fluctuations, supported by previous research. Additionally, this novel technique seeks to smooth PV power fluctuations and counteract EV demand patterns, resulting in a significant improvement in the quality of power delivered to the grid and reducing the cost. For simplicity, the main contributions are summarized below:

- Development of the PFS method for PV systems with a HESS with SC and VRFB.
- Implementation of innovative control strategies: PV fluctuations reduction strategy and peak demand reduction strategy for EVCS.
- Utilization of prediction to calculate EV demand and minimize grid impact through VRFB storage.
- Validation through experimental research and simulations in various operational situations and conditions.

The structure of the article is as follows: Section 2 initially defines the challenge of integrating renewable sources and mitigating fluctuations. Secondly, it addresses the potential impact of EVCS on the electrical grid. In Section 3, the proposed power smoothing method is detailed, based on two control strategies: a) PV fluctuation reduction strategy, and b) peak reduction strategy for EVCS. The specific analysis focuses on the hybrid combination of SC and VRFB. Section 4 presents the application through a case study with real charging station profiles for EVs, including the integration of the algorithm into the supervisory control and data acquisition system. In Section 5, the obtained results are analyzed in comparison to other smoothing methods, providing a comparative study under different climatic conditions over three representative days. This is accompanied by a sensitivity analysis and a comprehensive technical-economic study. Finally, potential future application fields are presented, and Section 6 concludes the article.

2. Problem definition

To achieve the proposed objective in this study, several perspectives and steps must be considered. Firstly, the reduction of PV fluctuations has a maximum allowed rate of 10 %/min, as certified by certain energy distribution companies [24]. To address faster fluctuations, SC are employed. Some studies propose installing lead-acid or lithium-ion BESSs alongside the PV system [36,37], while others suggest using SC banks or a combination of both [27,28]. However, the approach presented in the former studies is generally not advantageous, as the costs of BESS replacement may not generate sufficient revenue for power smoothing applications. On the other hand, the latter approach [27,28] shows more promise provided an appropriate energy control is implemented, and fluctuations are accurately classified based on their rate of change. This can be achieved through precise power fluctuation prediction, as demonstrated in this study. For this purpose, the "PV fluctuation reduction strategy" is presented, based on [12], considering PV and SC, and generating the reference power for SC ($P^{SC}{}_{ref}$).

Secondly, simultaneous reduction of electricity purchase from the grid during EVCS peak demands is addressed with the assistance of SC and VRFB. EVs are classified based on their intended purpose, including private vehicles, official vehicles, taxis, and buses [35]. In [38] the authors classify EV charging infrastructure into three levels: (i) level 1 and 2 residential charging, (ii) level 2 work and public place charging, and (iii) level 3 dc fast charging. In this study, the prediction of demand for public EVCSs considers only two criteria: private EVs and electric taxis (TEVs), as official EVs and electric buses typically have their own specialized charging facilities. To address this, the "peak reduction strategy for EVCS" is presented, based on [12], but considering VRFB

and the EV's demand (X_{EV}). Fig. 1 illustrates the schematic diagram of the proposed method and extensive experimental tests have been conducted in the microgrid laboratory at the University of Cuenca (CCTI-B). The proposed control system is executed through the SCADA system, and HESS components are interconnected to an alternating current (AC) bus, which is subsequently connected to the electrical grid.

3. Proposed PFS method

The proposed method is based on a combination of conventional algorithms RR and MA. This combined approach provides a robust and accurate power reference signal for the hybrid storage system (SC and VRFB), considering predictions of power fluctuations PV, EVCS, and energy exchange with the electrical grid. To achieve this, the proposed PFS method introduces two control strategies, which are described below:

3.1. PV fluctuation reduction strategy

In the first stage of this strategy, the ramp limit for the output power is set by calculating the PV power variation during a predefined time according to Eq. (1):

$$f_{pv}(t) = \frac{dp_t(t)}{dt} = \pm\left|\frac{p_t(t+1) - p_t(t)}{\Delta t}\right| \leq 10\%Pn \tag{1}$$

where $f_{pv}(t)$ is the PV power fluctuation calculated at two-time instants, p_t represents the instantaneous PV power at time t, and its derivative indicates the rate of change with respect to time, dt. This representation can be calculated as the PV power value $p_t(t+1)$ at a time $t+1$ within the time range Δt, typically within a 1-minute window. The obtained value is recommended to be within ±10 %/min of the nominal power of the installation Pn.

To reduce power fluctuations, it is necessary to identify peaks that surpass the threshold value. For this purpose, we employ a cluster-based machine learning technique to classify the fluctuations, and we explain this technique here. Considering each day, to categorize groups of positive and negative power fluctuations derived from Eq. (1). The correction method utilizes the k-means algorithm for clustering and the selection of representative days. The primary objective is to minimize the sum of squared distances, $\underset{Sf_{pv}}{minE}(\mu_i)$, for each fluctuation group from its cluster centroid. This process is executed through the following function, as defined in Eq. (2). The power fluctuation data is represented by vectors of real values in d dimensions (8640 per day): $\left\{f_{pv}(1), f_{pv}(2), \ldots f_{pv}(n)\right\}$. The k-means algorithm determines k clusters where the sum of distances of the data within each group, $Sf_{pv} = \left\{Sf_{pv}(1), Sf_{pv}(2), \ldots Sf_{pv}(k)\right\}$, is minimized to its centroid point μ_i.

$$\underset{Sf_{pv}}{minE}(\mu_i) = \underset{Sf_{pv}}{min}\sum_{i=1}^{k}\sum_{f_{pv}(j)\in Sf_{pv}(i)}\left\|f_{pv}(j) - \mu_i\right\|^2 \tag{2}$$

where Sf_{pv} are elements are the PV fluctuations $f_{pv}(j)$ represented by data vectors, μ_i are the centroid of k-means algorithm, k represent the total number of clusters or centroids.

In this way, the modulation coefficient (CC) can be established for the number of cycles required for the BESS optimization as the sum of the clusters k that exceed the ±10 % threshold and is calculated as the number of positive fluctuations $k_{\#positive}$ divided by the number of negative fluctuations $k_{\#negative}$ ($CC = k_{\#positive}/k_{\#negative}$). In the second stage of reducing PV fluctuations, the reference power for SC operation is determined using the MA method to predict the value $(\widehat{p}_t^{\,SC})$ as shown in Eq. (3).

$$\widehat{p}_t^{\,SC} = \frac{1}{NMA^{SC}}\sum_{t=1}^{NMA^{SC}} X_{t-NMA^{SC}+t-1} \tag{3}$$

This prediction represents the expected SC operation for the next time instant $(t+1)$ based on the current time (t). The prediction window is short-term, typically around 10 min, and can be adjusted based on the user-defined interval (NMA^{SC}). The choice of NMA^{SC} depends on the desired precision and the ramp rate of fluctuation, which in this case is 10 % per minute. In Eq. (3), the term $X_{t-NMA^{SC}+t-1}$ represents the predicted PV power values for a very short time interval from input vector X_t. Subsequently, using the RR method described in Eqs. (4)–(7), the energy storage variation in SC is calculated while considering the prescribed allowable ramp rate $\pm {R_{max}}^{SC}$ for a specific time interval Δt^{SC}. The efficiencies of charging and discharging, ${\eta_C}^{SC}$ and ${\eta_D}^{SC}$ respectively, are considered in these calculations. Additionally, the coefficient of modulation CC allocates the adjustment parameter based on a comprehensive cluster analysis of the charging/discharging cycles using the k-means algorithm as defined in Eq. (2). Ultimately, the reference power value for the SC system, denoted as ${P^{SC}}_{ref}$, is established through these computations [12]. This configuration allows optimizing the use of supercapacitors in the performance of charge/discharge cycles.

$${vs_t}^{SC} = max\left\{0, X_t - \left(p_t + P{\cdot}{R_{max}}^{SC}{\cdot}60{\cdot}\Delta t^{SC}\right)\right\} \tag{4}$$

$${sr_t}^{SC} = max\left\{0, \left(p_t + P{\cdot}{R_{max}}^{SC}{\cdot}60{\cdot}\Delta t^{SC}\right) - X_t\right\} \tag{5}$$

$$\Delta_{SOC_t^{SC}} = \frac{1}{NMS^{SC}}\sum_{t=1}^{NMS^{SC}}\left({\eta_C}^{SC}{\cdot}{vs^{SC}}_{t-NMS^{SC}+t-1} - \frac{1}{{\eta_D}^{SC}}{\cdot}{sr^{SC}}_{t-NMS^{SC}+t-1}\right) \tag{6}$$

$${P^{SC}}_{ref} = \widehat{p}_t^{\,SC} + CC{\cdot}\Delta_{SOC_t^{SC}} \tag{7}$$

where $\widehat{p}_t^{\,SC}$ is the SC reference power prediction value using the moving average method, NMA^{SC} represent the number of periods used to calculate the SC moving average, $X_{t-NMA^{SC}+t-1}$ is the predicted PV values for a very short time interval, ${vs_t}^{SC}$ is the power transferred from the photovoltaic panels to SC storage in period t (cut peaks), X_t is output power of the PV installation (without smoothing) at instant t, p_t is PV power value obtained in real time, P is the nominal power capacity of the PV system, Δt^{SC} represents SC time interval, ${sr_t}^{SC}$ is the power transferred from SC storage to the grid in period t (fill gaps), $\Delta_{SOC_t^{SC}}$ is the value of the average variation of power in SC storage, NMS^{SC} represents the number of periods used to calculate the variation in the energy contained in the SC storage, ${vs^{SC}}_{t-NMS^{SC}+t-1}$ is the power transferred from the PV panels to SC storage in very short time interval and ${sr^{SC}}_{t-NMS^{SC}+t-1}$.

3.2. Peak reduction strategy for EVCS

In this second strategy, the reference power for the VRFB is generated considering the reduction of PV fluctuations and the optimal energy management for the EVCS. To obtain the prediction of fluctuations, note that Eq. (8) is similar to (3), but with the difference that now the initial memory NMA^{VR} is calculated with respect to the VRFB instead of the SC. Likewise, the MA method is used, and consequently, the RR method is applied to limit fluctuations, which are commonly slower and beyond the reach of the SC, as represented in Eqs. (9)–(11).

$$\widehat{p}_t^{\,VR} = \frac{1}{NMA^{VR}}\sum_{t=1}^{NMA^{VR}} X_{t-NMA^{VR}+t-1} \tag{8}$$

$${vs_t}^{VR} = max\left\{0, X_t - \left(p_t + P{\cdot}{R_{max}}^{VR}{\cdot}60{\cdot}\Delta t^{VR}\right)\right\} \tag{9}$$

$${sr_t}^{VR} = max\left\{0, \left(p_t + P{\cdot}{R_{max}}^{VR}{\cdot}60{\cdot}\Delta t^{VR}\right) - X_t\right\} \tag{10}$$

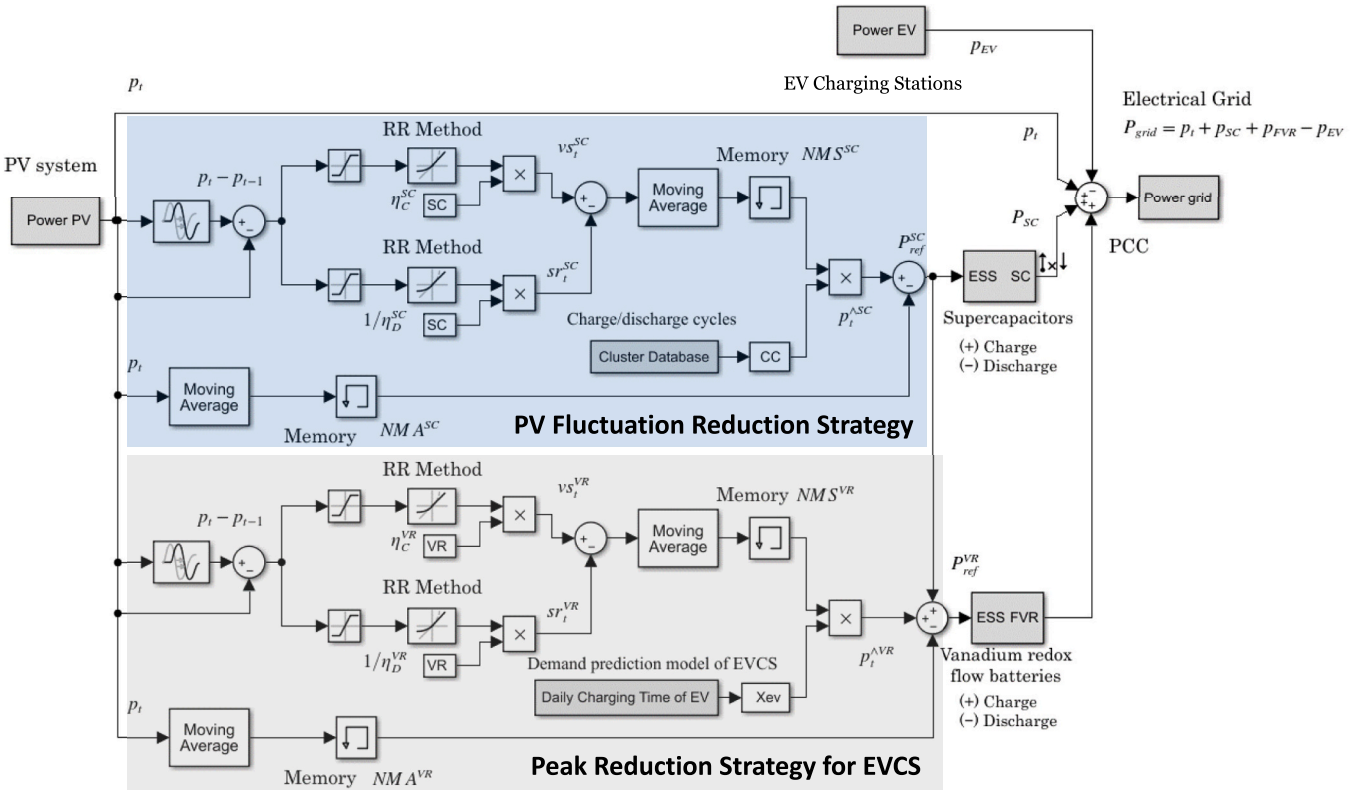

Fig. 2. Control diagram illustrating the proposed PFS algorithm.

$$\Delta_{SOC_t^{VR}} = \frac{1}{NMS^{VR}} \sum_{t=1}^{NMS^{VR}} \left({\eta_C}^{VR} \cdot {vs}^{VR}{}_{t-NMS^{VR}+t-1} - \frac{1}{{\eta_D}^{VR}} \cdot {sr}^{VR}{}_{t-NMS^{VR}+t-1} \right) \quad (11)$$

where $\widehat{p_t}^{VR}$ is the VRFB reference power prediction value using the MA method, NMA^{VR} is the number of periods used to calculate the VRFB moving average, $X_{t-NMA^{VR}+t-1}$ is the predicted PV values for a very short time interval in VRFB, ${vs_t}^{VR}$ is the power transferred from the PV panels to VRFB storage in period t (cut peaks), ${R_{max}}^{VR}$ is VRFB maximum ramp value control, Δt^{VR} is VRFB time interval, ${sr_t}^{VR}$ is the power transferred from VRFB storage to the grid in period t (fill gaps), $\Delta_{SOC_t^{VR}}$ is the value of the average variation of power in VRFB storage, NMS^{VR} represents the number of periods used to calculate the variation in the energy contained in the VRFB, ${\eta_C}^{VR}$ and ${\eta_D}^{VR}$ VRFB performance during the storage charge and discharge process respectively, ${vs}^{VR}{}_{t-NMS^{VR}+t-1}$ represents the power transferred from the PV panels to VRFB storage in very short time interval, ${sr}^{VR}{}_{t-NMS^{VR}+t-1}$ is the power transferred from the PV panels to VRFB storage in very short time interval.

Subsequently, to generate the reference power for the VRFB (${P^{VR}}_{ref}$), it is necessary to consider the coefficient of the demand prediction model of the EVCS, (X_{EV}). This coefficient assigns the adjustment parameter and is calculated using Eq. (13). Then, to reduce the impact of EVs, an estimation of the EV demand is used through the charging demand characteristics of EVs as expressed in Eq. (15).

By considering various factors affecting the location of EVCSs, a relationship between quantitative factors and the mathematical model is established, ultimately obtaining a reasonable and reliable scale for the EVCS expressed in Eq. (13). It is worth noting that the ${R_{max}}^{VR}$ values differ for each storage system. To leverage greater energy accumulation in the VRFB, its RR must be set higher $\pm {R_{max}}^{VR} \gg \pm {R_{max}}^{SC}$. Finally, the reference power value of the VRFB (${P^{VR}}_{ref}$) is established, considering the mitigation of SC fluctuations already executed in the previous strategy ($\Delta_{SOC_t^{VR}} + {P^{SC}}_{ref}$) and the power of the EVCS P_{EV} as shown in Eq. (12) [35]. This configuration enables effective control of SOC for VRFB. Consequently, it facilitates regenerative energy accumulation to mitigate the impact of peaks generated during vehicle charging on the grid. Moreover, it allows for the adjustment of EVs demand prediction with characteristic tuning parameters tailored to each specific case.

$$P^{VR}{}_{ref} = \widehat{p_t}^{VR} + X_{EV} \cdot \Delta_{SOC_t^{VR}} + P^{SC}{}_{ref} - P_{EV} \quad (12)$$

Subsequently, to generate the reference power for the VRFB (${P^{VR}}_{ref}$), it is necessary to consider the coefficient of the demand prediction model of the EVCS, X_{EV}. This coefficient assigns the adjustment parameter and is calculated using Eq. (13). Then, to reduce the impact of EVs, an estimation of the EV demand is used through the charging demand characteristics of EVs as expressed in Eq. (15) [35].

$$X_{EV} = M_{EV} \times \lambda_{EV} \times P_{EV} \times \gamma_{EV} \quad (13)$$

where X_{EV} the demand for charging power (kVA) of EVs, M_{EV} is connection coefficient, which is between 0 and 1; λ_{EV} is the current forecast number of EVs, P_{EV} is the power of a single EV, and γ_{EV} is the EV charging time per day.

$$\gamma_{EV} = \frac{SY/T_{EV}}{SD} \quad (14)$$

where γ_{EV} is actual charging time of EV per day, SY is Average annual mileage of an EV (km), T_{EV} is the number of days an electric vehicle drives per year, SD is the range of electric vehicle battery (km). In the event that the number of Electric Vehicles (EVs) is unavailable, or a prediction is desired, the following equation proposed by [35] can be utilized.

$$F_T = F_{T-1} + p(m - F_{T-1}) + q\frac{F_{T-1}}{m}(m - F_{T-1}) \quad (15)$$

where F_T is cumulative consumption until T, F_{T-1} is cumulative consumption before $T-1$ m is maximum coefficient of sales on the market.

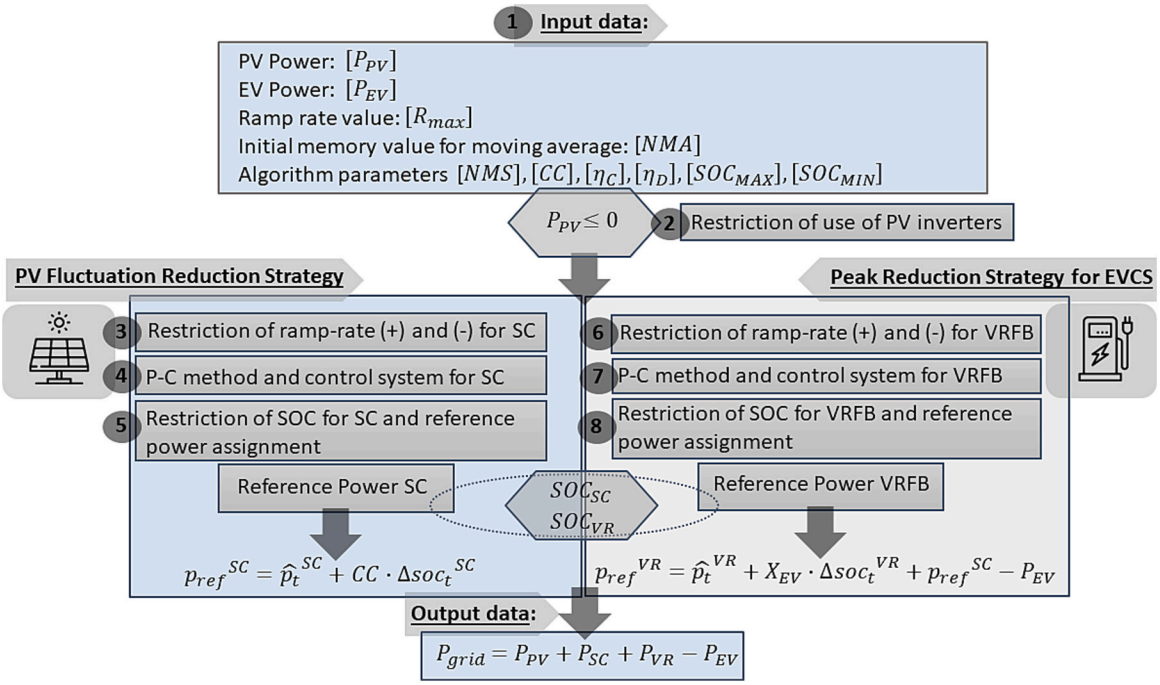

Fig. 3. Flowchart illustrating the novel proposed methodology.

p is innovation coefficient, which represents the number of people who buy products that are influenced by other consumers; q is the imitation coefficient, which represents the number of people who buy products [35].

In the Fig. 2, the process of the PFS Method controller is summarized. The input values include the power of the PV system and the power of the EV. To establish reference values for the SC and VRFB, two strategies are generated: the PV fluctuations reduction strategy, as outlined by Eqs. (3)–(7). The controller, previously proposed by the authors in [12], has been integrated with the EVCS, following the same concept of determining a lower ramp rate, as defined by Eqs. (8)–(15).

3.3. Computational implementation of the proposed algorithm

This section provides a detailed explanation and implementation of the method. Fig. 3 shows the flowchart, illustrating the control algorithm steps. Pseudocode for each step is presented below. The PV fluctuation reduction strategy (items 3–5) and peak reduction strategy for EVCS (items 6–8) are included:

1. Data Input. Real-time power data is collected for each system, and the constant adjustment parameters of the algorithm are entered.
2. Restriction on PV inverter usage. To prevent the use of storage systems, the reference power for SC and VRFB is set to zero.
3. RR restriction for SC. The allowable upper RR is limited to 10 % of the PV nominal power.
4. Predictor corrector (P—C) method and control system for SC. The prediction and correction method are applied using SC [12].

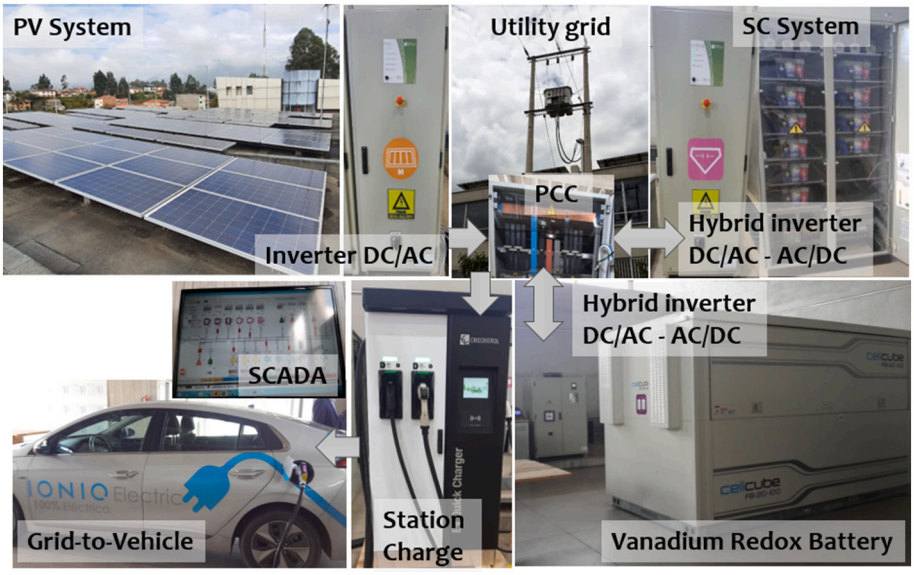

Fig. 4. Pictorial representation of the laboratory equipment (CCTI-B) used for the experiments of the proposed PFS method.

5. SOC restriction for SC. Maximum and minimum values are established for the SOC of SC. When the set range is exceeded, VRFB is combined with SC.
6. RR restriction for VRFB. The allowable upper RR is limited to 1 % (adjustable heuristically) of the PV nominal power for energy utilization.
7. P—C method and control system for VRFB. The prediction and correction method are applied using VRFB. SC initially absorbs and delivers energy with very fast response, combined with VRFB to improve the PV system's output signal and energy accumulation for EVSC.
8. SOC restriction for VRFB. Maximum and minimum values are established for the SOC of VRFB.

Pseudocode

1. Data Input
1.1. Constant data: P, R_{max}^{SC}, Δt^{SC}, NMA^{SC}, NMS^{SC}, η_C^{SC}, η_D^{SC}, CC, SOC_{min}^{SC}, $SOC\ _{max}^{SC}$, $R\ _{max}^{SC}$, Δt^{SC}, R_{max}^{VR}, Δt^{VR}, NMA^{VR}, NMS^{VR}, η_C^{VR}, η_D^{VR}, SOC_{min}^{VR}, $SOC\ _{max}^{VR}$
1.2. Variable data: p_t, X_t, SOC^{SC}, SOC^{VR}, X_{EV}, P_{EV}
2. Restriction of use of PV inverters:
2.1. If $p_t \leq 0$
2.2. $P_{ref} = 0$
2.3. End if
3. Restriction of ramp-rate (+) and (-) for SC
3.1. If $|p_t - p_{t-1}| > P \cdot R_{max}^{SC} \cdot 60 \cdot \Delta t^{SC}$
3.2. If $p_t - p_{t-1} > 0$
3.3. $X_t = p_{t-1} + P \cdot R_{max}^{SC} \cdot 60 \cdot \Delta t^{SC}$
3.4. Else $X_t = p_{t-1} - P \cdot R_{max}^{SC} \cdot 60 \cdot \Delta t^{SC}$
3.5. End if
3.6. End if
4. PV Fluctuation Reduction Strategy for SC
Data processing:
Reference PV power prediction value using the MA method.
4.1. $\hat{p}_t{}^{SC} = \frac{1}{NMA^{SC}} \sum_{t=1}^{NMA^{SC}} X_{t-NMA^{SC}+\tau-1}$
*NMA^{SC} initial memory time required (10 min) for SC
Power transferred from the PV panels to storage in period t (cut peaks)
4.2. $vs_t{}^{SC} = max\{0, X_t - (p_t + P \cdot R_{max}^{SC} \cdot 60 \cdot \Delta t^{SC})\}$
Power transferred from storage to the grid in period t (fill gaps)
4.3. $sr_t{}^{SC} = max\{0, (p_t + P \cdot R_{max}^{SC} \cdot 60 \cdot \Delta t^{SC}) - X_t\}$
Value of the average variation of power in storage
4.4. $\Delta soc_t{}^{SC} = \frac{1}{NMS^{SC}} \sum_{t=1}^{NMS^{SC}} (\eta_C^{SC} \cdot vs^{SC}{}_{t-NMS^{SC}+\tau-1} - \frac{1}{\eta_D^{SC}} \cdot sr^{SC}{}_{t-NMS^{SC}+t-1})$
*NMS^{SC} initial memory time required (5 min) for SC
*Charge and discharge efficiency parameters η_C^{SC} and η_D^{SC} for SC
Reference power to SCs
4.5. $p_{ref}{}^{SC} = \hat{p}_t{}^{SC} + CC \cdot \Delta soc_t{}^{SC}$
*CC correction intensity modulation coefficient [0-5]
5. Restriction of SOC for SC and reference power assignment
5.1. If $SOC_{min}^{SC}, \leq SOC_{SC} \leq SOC\ _{max}^{SC}$
5.2. $P_{SC} = p_{ref}{}^{SC}$
5.3. Else $P_{SC} = 0$
5.4. End if
6. Restriction of ramp-rate (+) and (-) for VRFB
6.1. If $|p_t - p_{t-1}| > P \cdot R_{max}^{VR} \cdot 60 \cdot \Delta t^{VR}$
6.2. If $p_t - p_{t-1} > 0$
6.3. $X_t = p_{t-1} + P \cdot R_{max}^{VR} \cdot 60 \cdot \Delta t^{VR}$
6.4. Else $X_t = p_{t-1} - P \cdot R_{max}^{VR} \cdot 60 \cdot \Delta t^{VR}$
6.5. End if
6.6. End if
7. Peak Reduction Strategy for EVCS and control system for VRFB
Data processing:
Reference PV power prediction value using the MA method.
7.1. $\hat{p}_t{}^{VR} = \frac{1}{NMA^{VR}} \sum_{t=1}^{NMA^{VR}} X_{t-NMA^{VR}+\tau-1}$
*NMA^{VR} initial memory time required (≥20 min) for VRFB
Power transferred from the PV panels to storage in period t (cut peaks)
7.2. $vs_t{}^{VR} = max\{0, X_t - (p_t + P \cdot R_{max}^{VR} \cdot 60 \cdot \Delta t^{VR})\}$
Power transferred from storage to the grid in period t (fill gaps)
7.3. $sr_t{}^{VR} = max\{0, (p_t + P \cdot R_{max}^{VR} \cdot 60 \cdot \Delta t^{VR}) - X_t\}$
Value of the average variation of power in storage
7.4. $\Delta soc_t{}^{VR} = \frac{1}{NMS^{VR}} \sum_{t=1}^{NMS^{VR}} (\eta_C^{VR} \cdot vs^{VR}{}_{t-NMS^{VR}+\tau-1} - \frac{1}{\eta_D^{VR}} \cdot sr^{VR}{}_{t-NMS^{VR}+t-1})$
*NMS^{VR} initial memory time required (5 min) for VRFB
*Charge and discharge efficiency parameters η_C^{VR} and η_D^{VR} for VRFB
Reference power to VRFB
7.5. $p_{ref}{}^{VR} = \hat{p}_t{}^{VR} + X_{EV} \cdot \Delta soc_t{}^{VR} + p_{ref}{}^{SC} - P_{EV}$
*X_{EV} demand prediction model of charging stations
8. Restriction of SOC for VRFB and reference power assignment
8.1. If $SOC_{min}^{VR}, \leq SOC_{VR} \leq SOC\ _{max}^{VR}$
8.2. $P_{VR} = p_{ref}{}^{VR}$
8.3. Else $P_{VR} = 0$
8.4. End if

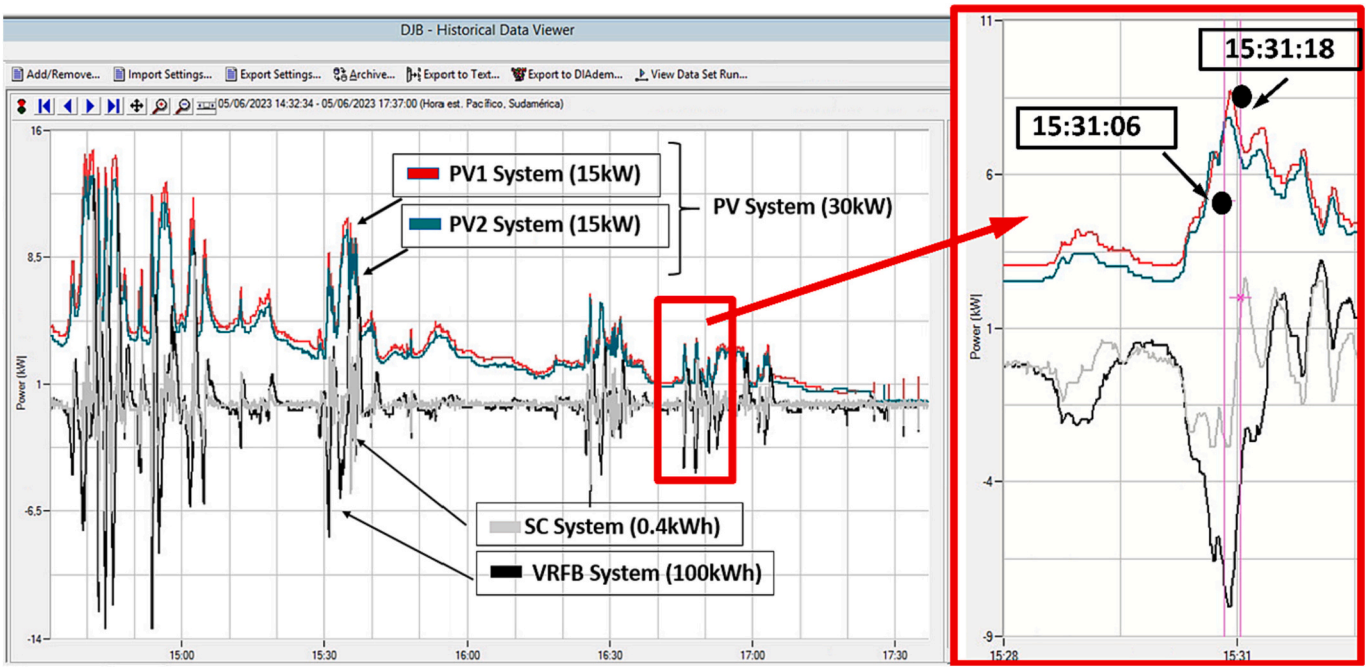

Fig. 5. Screenshot of the SCADA system. (a) Implementation of the proposed algorithm. (b) System response time.

Table 1
Technical specifications of the equipment employed in the experiment.

Equipment description	Model	Cells/ modules	Operating voltage	Energy	Capital cost
PV system 1 (15 kWp)	Monocrystalline	60 (15 × 4)	150 Vdc–450 Vdc/230 Vac	Up to 50 kWh	870 (USD/ kW) [39]
PV system 2 (15 kWp)	Polycrystalline	60 (15 × 4)	150 Vdc–450 Vdc/230 Vac	Up to 50 kWh	857 (USD/ kW) [39]
SC	Maxwell BMOD-0130	10 cells	560 Vdc/ 230Vac	0.4 kWh	27.5 (USD/ Wh) [12]
VRFB	Cell Cube FB 10–100	1 integrated module	48 Vdc/ 127Vac; 230Vac	100 kWh	700 (USD/ kWh) [12]
Utility grid	N/A	N/A	230 Vac	N/A	

Table 2
Primary technical details of the analyzed EVs.

EV model	Type	Battery capacity	Autonomy electric range	Regenerative braking
BYD E5 300	BEV	60 kWh	400 km	Yes
IONIQ EV	BEV	39 kWh	300 km	Yes
KIA SOUL EV	BEV	64 kWh	450 km	Yes

4. Case study

4.1. Implementation of the PFS in the experimental platform (CCTI-B)

The CCTI-B served as the experimental platform for validating the power smoothing method. Fig. 4 illustrates the equipment configuration, with further details in [28]. To ensure efficient communication, an Ethernet Modbus TCP/IP connection and MATLAB code were designed for seamless interaction between devices and the SCADA system, enabling control and monitoring through a MATLAB and LabVIEW interface [29]. Fig. 5 shows the real-time implementation of the hybrid storage system, effectively smoothing both PV and power grid. The proposed algorithm operates autonomously with minimal delays (500 ms). The primary technical specifications of the system components being tested are presented in Table 1. Similarly, Table 2 presents the technical details of the EVs employed in this experiment. Three EVs were utilized to ensure comparative results and mitigate any potential imperfections that may arise.

4.2. Experimental validation of energy storage systems and electric vehicles

Experimental tests on HESS and EVCSs validate their real-time functionality and response, controlled by the SCADA system using MATLAB. Fig. 6(a) shows VRFB charge and discharge tests. The state of charge of the VRFB SOC_{VRFB} can be calculated based on the operating voltage as indicated in Fig. 6 where the operating range for each cluster A, B is between 42.7 V and 62.89 V, which indicates an approximate variation of 20 V in energy storage in concentration of vanadium ions and protons. The VRFB can be regularly deep discharged (0 % charge level) without damaging itself. However, as for all electrochemical batteries, output power (kW) and capacity (kWh) may be affected by temperature and other operating conditions [40], while Fig. 6(b) depicts SC charge and discharge performance at different power settings. Response times, <500 ms, align well with mathematical models, ensuring reliable practical operation. The time of energy use by SCs is reduced in the order of seconds, however they have a very fast response to large amounts of energy, which is their main advantage within HESS.

Results for various EV models, including the KIA SOUL, are presented in Fig. 7(a), evaluating power smoothing with semi-fast and fast chargers. Fig. 7(b) illustrates the power demand of EV charging, denoted as (X_{EV}), utilizing Eqs. (16) and (17). This characterization is based on EVs with an average annual mileage of $SY = 200.000$ km, estimating $T_{EV} =$ 300 days of EV operation per year, and an electric vehicle battery range $SD = 200$ km per charge. The power of each EV ($P_{EV} = 45$ kW) with a charging time of 30 min. The graph explores a range of $\lambda_{EV} = 1$ to 10 EVs, and the connection coefficient M_{EV} is varied from 0.1 to 1. These analyses provide insights into charging strategies and the real-world

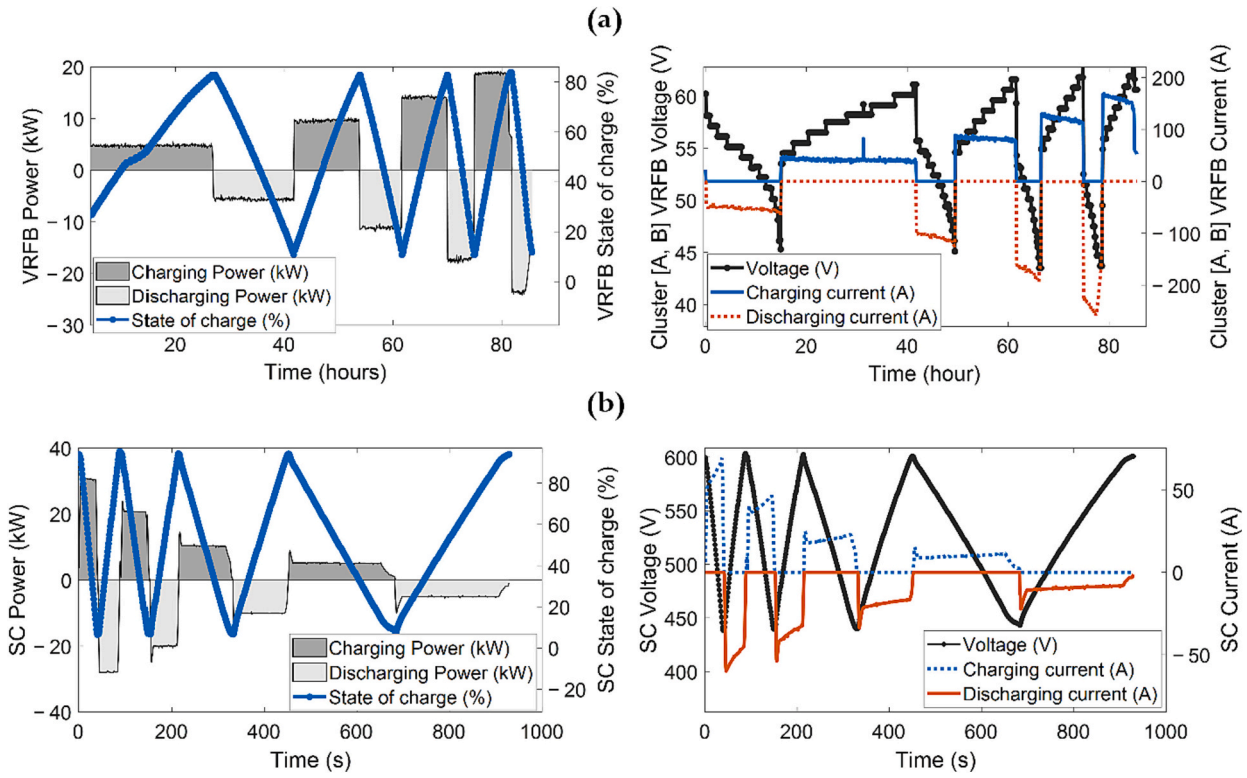

Fig. 6. (a) Experimental of the VRFB under various power settings. (b) Experimental tests of the SC under various power settings.

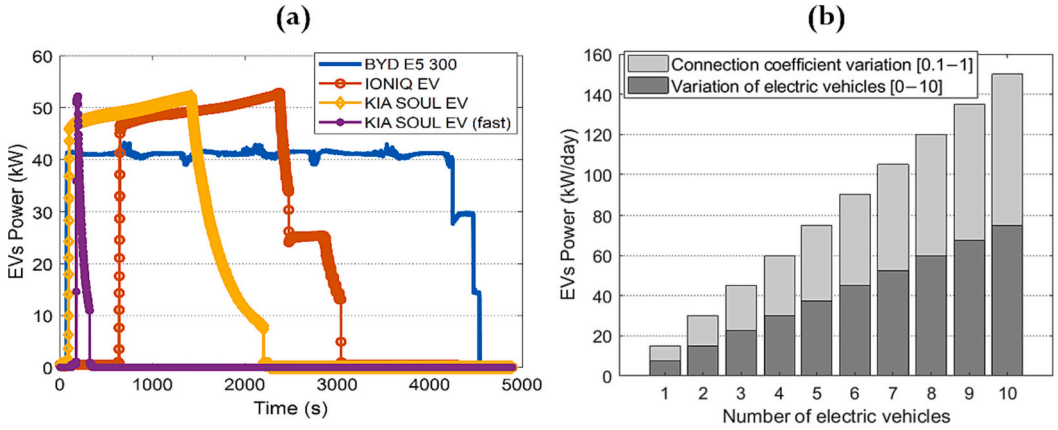

Fig. 7. (a) Results of the charge/discharge experiment for various illustrative EV charging profiles 0 to 100 %. (b) Calculation of EV charging power demand.

performance of EVs.

Table 3 summarizes the adjustment parameters of the case study for the implementation of the proposed algorithm as established in Section 3.3.

5. Results and discussions

5.1. Power smoothing results

This section presents the results of the proposed PFS method. Initially, the PV/EVCS system's conventional behavior connected to the grid is shown in Fig. 8(a), without any power smoothing methods or ESS (SC and VRFB). In the red box, it becomes evident that the PV power alone cannot fully meet the demand of the connected EVs. As a result, additional power from the grid ($P_{GRID} \geq 0$) is required to fulfill the EVs' demand. Moreover, the PV power fluctuations exceed the maximum allowed RR (10 %/min), causing disturbances in the grid throughout a typical day.

To address this issue, Fig. 8(b) demonstrates the application of the PFS method for the same study day, now considering the HESS (SC + VRFB). In the red box, it can be observed that the power sent to the grid ($P_{GRID} = 0$) is skillfully smoothed, exhibiting a RR that remains below 1 %/min of the nominal PV power. To achieve this, the SC actively contributes by providing reference power (P_{SC}), guided by the PFS algorithm, while the integration of VRFB (P_{VR}) notably enhances the power output delivered to the grid (P_{GRID}), assisting the SC in peak reduction and satisfying the EV demand. As a result, the algorithm's capability to effectively mitigate PV fluctuations at 1 %/min is evident, harnessing this control strategy to minimize the adverse impact of EVCS.

In pursuit of enhanced efficiency and optimal sizing of VRFB and SC, the algorithm maintains the VRFB power reference ($p_{ref}{}^{VR}$) at approximately 50 % of the VRFB state of charge (SOC_{VR}). This approach ensures

Table 3
Adjustment parameters for the control algorithm.

Description	Symbol	Parameter value	Considerations
Charging time of EV	Δt_{EV}	30 min	Semi-rapid or rapid charger type
SC time interval	Δt^{SC}	1 min	
VRFB time interval	Δt^{VR}	1 min	
SC performance during the storage charge process	η_C^{SC}	95 %	Validate with experimental tests
SC performance during the storage discharge process	η_D^{SC}	96 %	Validate with experimental tests
VRFB performance during the storage charge process	η_C^{VR}	90 %	Validate with experimental tests
VRFB performance during the storage discharge process	η_D^{VR}	92 %	Validate with experimental tests
SC reference power correction intensity modulation coefficient	CC	[0–5]	Previous analysis with fluctuation cluster
SC Maximum Ramp Value Control	R_{max}^{SC}	10 % × P	Allowed ramp-rate according to nominal power
VRFB Maximum Ramp Value Control	R_{max}^{VR}	1 % × P	Allowed ramp-rate according to nominal power
SC minimum state of charge	SOC_{min}^{SC}	0–5%	Requires initial preload
SC maximum state of charge	SOC_{max}^{SC}	95 %–100 %	Set by manufacturer
VRFB minimum state of charge	SOC_{min}^{VR}	0–5 %	Set by manufacturer
VRFB maximum state of charge	SOC_{max}^{VR}	98%–100 %	Set by manufacturer
Nominal power of the renewable photovoltaic system	P	30 kW	
Number of periods used to calculate the SC moving average	NMA^{SC}	10 min	Time window for smoothing 10 %
Number of periods used to calculate the variation in the energy contained in the SC storage	NMS^{SC}	5 min	Time window for smoothing 10 %
Number of periods used to calculate the VRFB moving average	NMA^{VR}	20 min	Time window for smoothing 1 %
Number of periods used to calculate the variation in the energy contained in the VRFB storage	NMS^{VR}	20 min	Time window for smoothing 1 %
Average annual mileage of an EV (km)	SY	200.000 km	Estimated value of EV models
EV connection coefficient	M_{EV}	0.8	Estimated value of EV models
Number of days an electric vehicle drives per year	T_{EV}	300	Estimated value of EV models
Range of EV battery (km)	SD	200 km	Estimated value of EV models
Current forecast number of EVs	λ_{EV}	5	Range of VE used by CS

that the VRFB system is sufficiently equipped to handle the impact associated with P_{EV} and the PV fluctuations that the SC cannot cover throughout the day, regardless of specific time frames. Additionally, the charging and discharging states of VRFB are autonomously regulated by $\left(p_{ref}{}^{VR}\right)$ in response to PV fluctuations, guaranteeing seamless compensation. This logic prevents unnecessary operation of the SC, as it is backed up by VRFB. This storage system SOC control strategy has been explained in steps 5 and 8 of the flowchart and pseudocode.

The power required for charging the EV averages $P_{EV} = 50$ kW, with an accumulated energy of 20 kWh. This energy needs to be supplied by the grid and the PV generation during the hours of the charging station's operation. In other words, $P_{GRID} = P_{PV} - P_{EV}$. In the strategy formulation, the contribution from the grid is minimized to zero due to the contribution provided by the ESS: $P_{GRID} = P_{PV} + P_{SC} + P_{VR} - P_{EV}$. Consequently, the mitigation of PV fluctuations is significantly reduced to <1 %/min, minimizing the direct impact of EVCS on the grid. It is worth noting that the SOC control for the VRFB is directly determined by a hybrid control algorithm combined with the SC. This hybrid approach allows for an oscillatory range of charging and discharging periods close to 50 % to address variable disturbances effectively. In Fig. 9(a), the spectral analysis of the smoothed signal with respect to PV power shows a significant reduction of 30 dB in the analysis range. The reduction in fluctuations at this stage maintains values below 1 %/min, facilitating the appropriate control of SC and VRFB within the specified maximum and minimum SOC ranges. This is achieved through the hybrid combination of these rapid and robust systems. Moving on to Fig. 9(b), the RR analysis from Eq. (1) is presented, examining three days: little cloudiness, clear day, and semi-clear day. Various RR percentages per minute are analyzed, projecting energy utilization below 10 % for energy storage and EVCS usage. The accumulated energy within this range allows for an additional 10 kWh to be generated, which can be stored while reducing the RR to as low as 1 % using the proposed method.

Therefore, the Table 4 presents a comparison of energy purchased from the grid under three different weather conditions. It shows the total daily energy generated by the PV system in kWh, the energy consumed by EV to charge them from 0 to 100 % in kWh, the PV energy used to charge the EVs in kWh, and the percentage of this energy relative to the total daily PV energy. In each condition, it is evident how the amount of energy purchased from the grid varies based on PV energy generation and EVCSs demand, highlighting the system's efficiency in different weather scenarios.

5.2. Comparison with other methods of power smoothing

5.2.1. Smoothing response analysis

This section compares the novel proposed method with two commonly used methods (MA and RR) as shown in Fig. 10(a). The MA method averages current power fluctuations without considering any prediction, leading to an exaggerated output signal. In contrast, the RR method only applies the ramp limit without considering the energy reserve for the ESS, unlike the proposed PFS method, potentially causing oversizing of the HESS. Fig. 10(b) illustrates that the proposed algorithm compensates the power profile of the EVCS directly with the VRFB, resulting in negative power curves if $f_{pv}(t) < P_{EV}$. The SOC is optimized for the SC and VRFB through predictive fluctuation analysis, as depicted in Fig. 11. The novel PFS method ensures optimized operability of the SC without erratic behavior observed in other power smoothing methods. The VRFB assists by providing energy during periods of lower power demand, enhancing the SC system's performance. These findings highlight the superiority of the proposed strategies over the commonly used methods, showcasing the effectiveness of energy accumulation analysis in SC and VRFB systems.

The comparative analysis in Fig. 12 demonstrates that the proposed PFS method outperforms the RR and MA methods in smoothing the PV power signal while staying within the 10 %/min limit. While all three methods meet the RR requirement, PFS achieves better power smoothing, thanks to its predictive capabilities and real-time correction strategies. The RR method lacks energy reserve management and response to rapid fluctuations, leading to potential oversizing and inadequate performance. Similarly, the MA method introduces averaging errors and delayed response times, making it less efficient in handling dynamic power profiles.

5.2.2. Analysis under different weather conditions

The PV system's daily power generation can exhibit unpredictability due to the intermittent nature of cloud cover. The comparison with various weather conditions is depicted in Fig. 13, where a comprehensive evaluation is performed by comparing the outcomes obtained with the MA and RR methods. It is important to note that during periods of negative power output ($P_{PFS} \leq 0$), the VRFB play a crucial role in

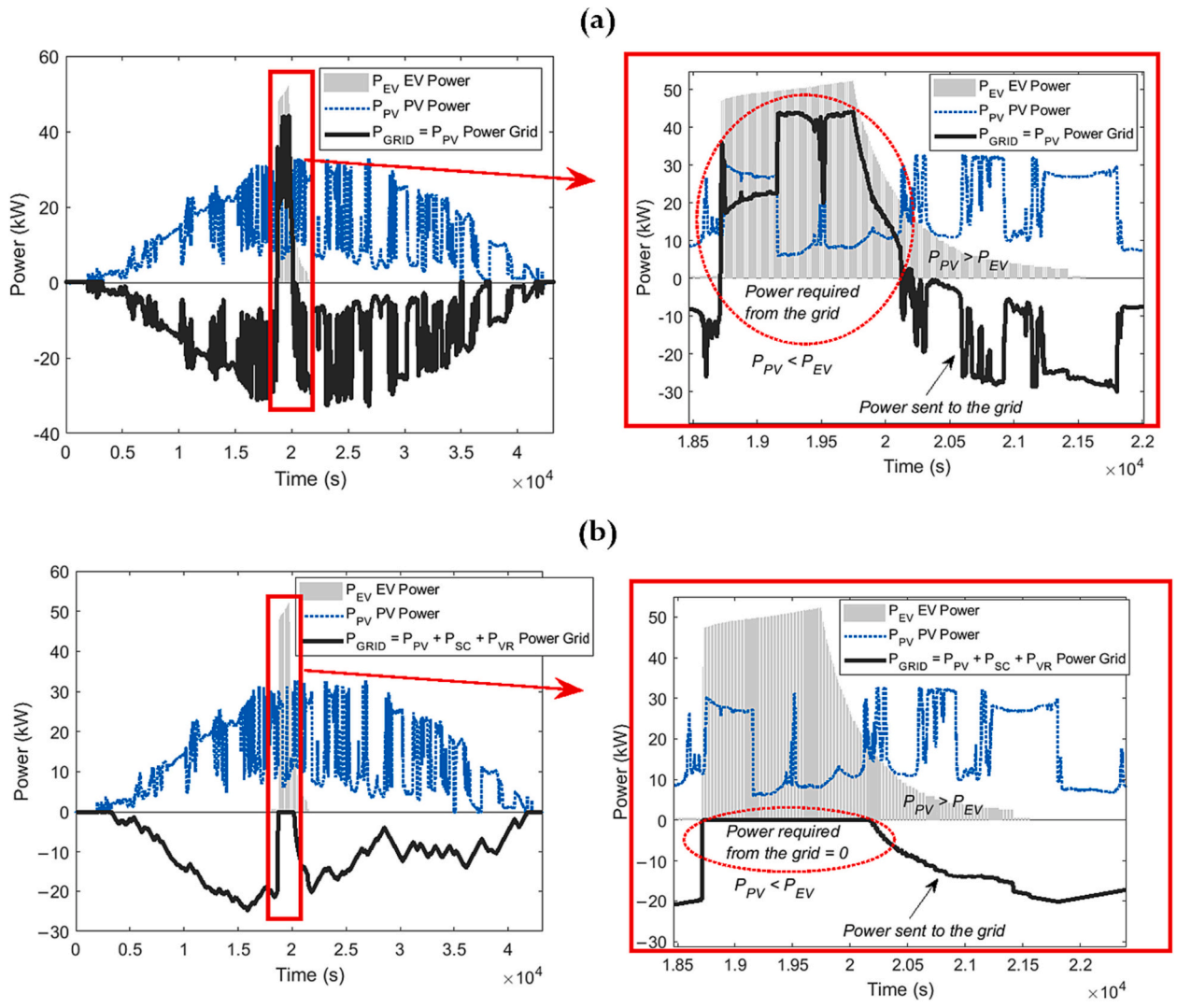

Fig. 8. (a) Results of the power output to the grid from the PV energy source without any smoothing or filtering applied. (b) Power smoothing of the output sent to the grid employing the newly proposed method.

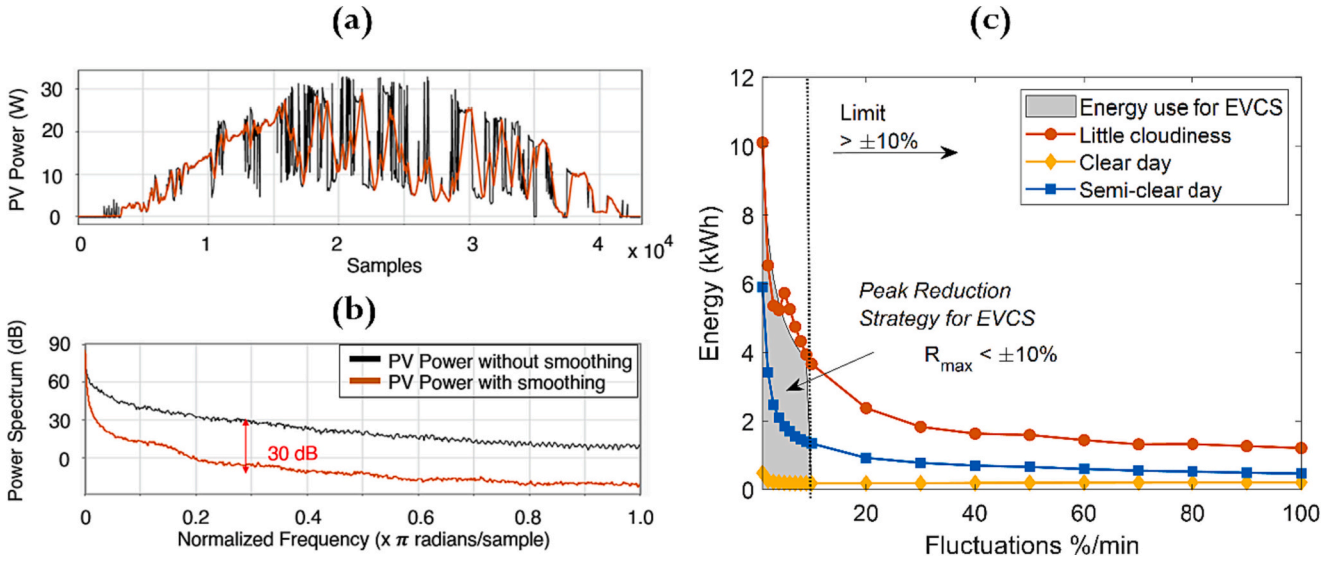

Fig. 9. Comparison analyses for power smoothing methods: (a) PV Power (kW), (b) Spectral (dB), (c) Limit ramp rate (%).

Table 4
Comparison of energy purchased from the grid.

Weather condition	Total daily PV energy (kWh)	EV energy (kWh) 0–100 %	PV-EV energy (kWh)	%
Little cloudiness	132.63	20.40	10.50	51.49
Clear day	181.63	20.40	8.22	40.29
Semi-clear day	125.83	20.40	8.35	40.95

supporting the system. This contribution is facilitated by the implementation of the peak reduction strategy for EVCS, which optimizes the distribution of energy required by the EVs based on their respective SOC.

By analyzing the comparative results, it becomes evident that the proposed method effectively mitigates the adverse impact of unpredictable PV generation, thereby enhancing the overall performance and reliability of the system. The utilization of VRFB in conjunction with the (peak reduction strategy for EVCS) demonstrates its efficacy in addressing the dynamic energy demands and fluctuations encountered in PV systems, particularly in scenarios characterized by varying cloud cover conditions In Fig. 13(a), a significant contribution from the SC and VRFB is evident due to a high index of fluctuations present on a day with little cloudiness. In contrast, on a clear day shows in Fig. 13(b), there is less demand for the contribution from the VRFB. Similarly, in Fig. 13(c), the contribution from the SC helps mitigate 10 % of the fluctuations. However, in all the aforementioned cases, the PV generation is lower than the power required for charging the EV, i.e., $P_{PV} < P_{EV}$. Consequently, the contribution from the VRFB must be immediate, providing a very high energy density of 20 kW during the EV charging period.

In summary, the Table 5 presents a comparison of different methods based on specific criteria. The first column represents the inclusion of a fast response with high power density in each method, denoted by "X" for those methods that meet this requirement. The second column indicates whether the method offers unlimited cycles of operation, and again, "X" signifies the presence of this characteristic. The third column highlights whether the method imposes a RR limitation of 10 %/min to control fluctuations, and the fourth column indicates if the method can supply energy to EVCS. From the Table 4, it can be observed that the PV + SC combination meets the criteria of fast response and high-power density, as well as offering unlimited cycles of operation. However, it

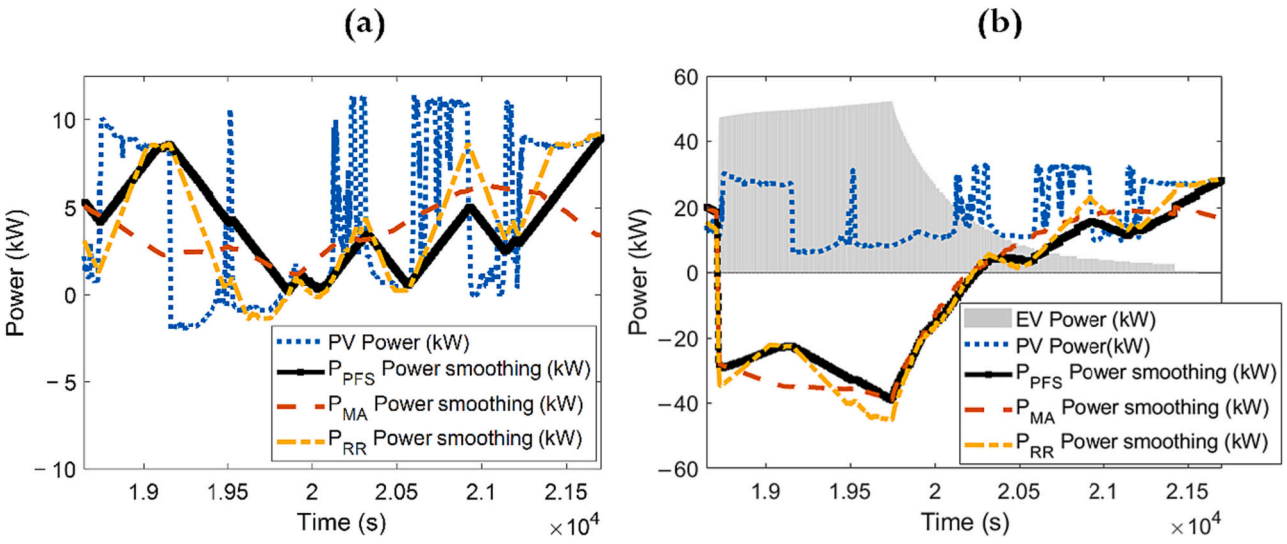

Fig. 10. Comparative analysis of MA, RR and PFS methods. (a) Input signal PV Power section. (b) Charging profile for EVCS.

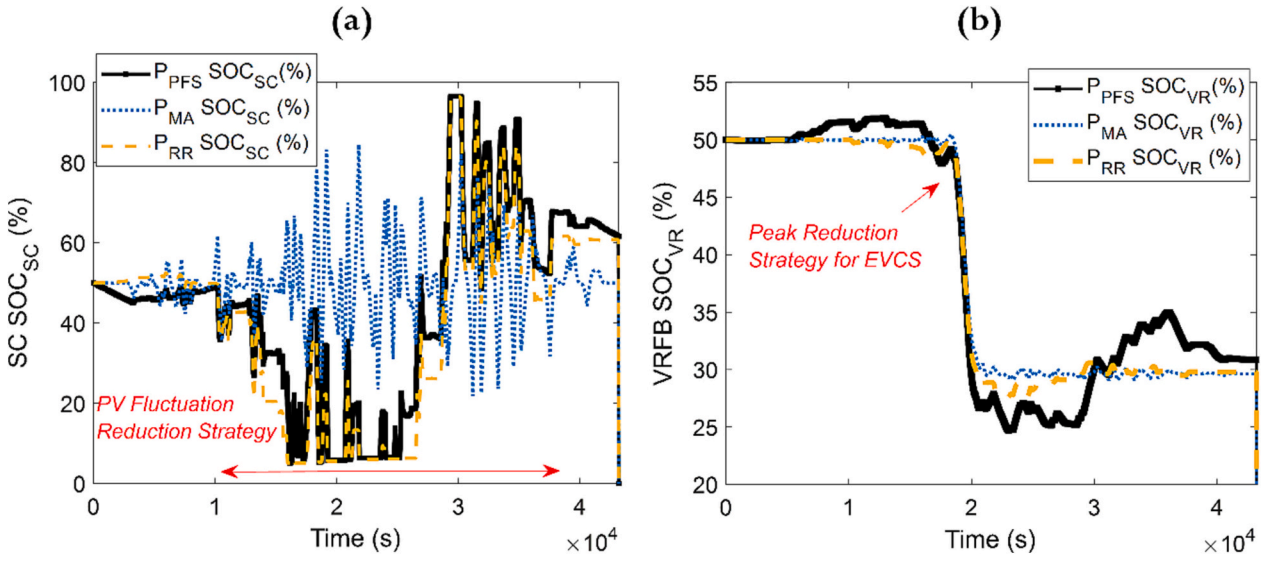

Fig. 11. Comparative analysis of MA, RR and PFS methods. (a) SOC for SC (b) SOC for VRFB.

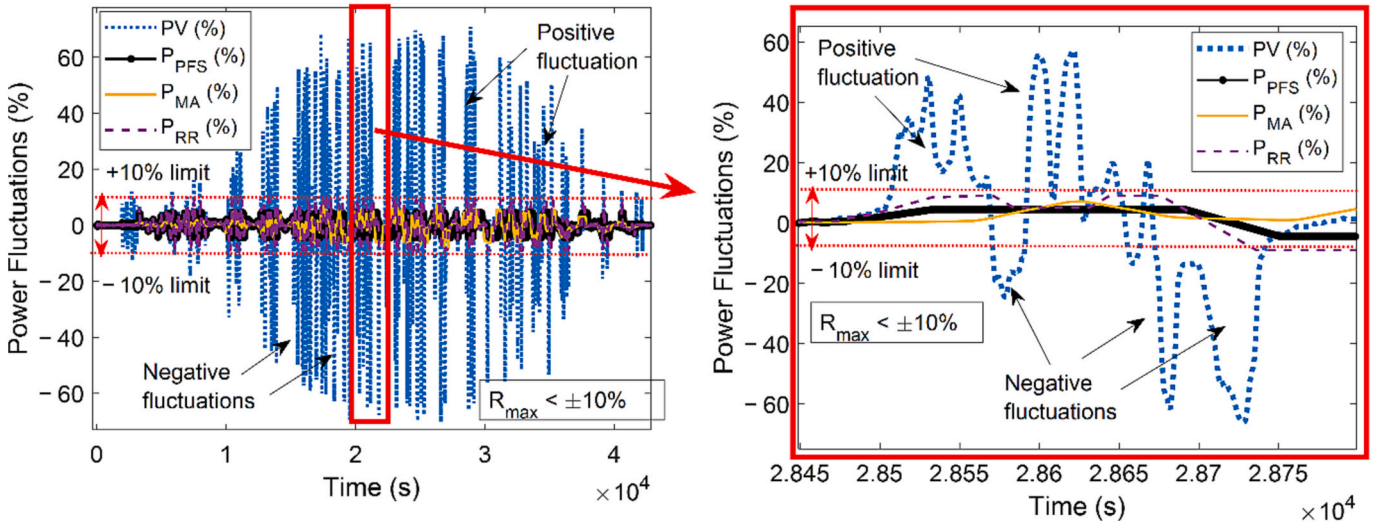

Fig. 12. Comparative analysis of power smoothing methods.

requires a substantial SC capacity, which can be a drawback. The PV + VRFB combination fulfills the rapid response, unlimited cycles, and RR limitation criteria. On the other hand, the PV + SC + VRFB method satisfies all the mentioned criteria, making it a comprehensive and effective solution for power smoothing and EVCS energy supply.

5.2.3. Analysis of noise and disturbance signals

Noise signals in control systems are usually common due to the different factors and electronic devices that make up power inverters and controllers. This section specifically analyzes the response of the controller under these effects. As observed in the previous figures, when starting and ending the PV generation stage, a small noise is produced in the PV power signal as a result of the power inverter starting. These values are usually very short-lived until the ideal MPPT (Maximum Power Point Tracking) value is updated. This defect is explained in Fig. 14(a) below, where the signal value can reach up to 4 kW during 1 s of recording. However, the proposed controller allows effective regulation up to a range of 0.2 kW and for lower values it returns the value of zero. In this way, the inappropriate use of ESS systems against this type of defective signals is regulated.

In addition, Fig. 14(b) shows the response of the controller to generator disturbances in long and short periods of time. It should be noted that the PFS controller begins its configuration with a vector of pre-registered values, therefore for disturbances that exceed 5 min it requires a readjustment in NMS^{SC} as indicated in Table 3. On the contrary, for disturbance generated in periods <5 min, the controller has an optimal response that does not affect the output signal. Likewise, the amplitude of the disturbance is not relevant since the algorithm focuses on smoothing the output signal. In both cases, prior to the implementation of the algorithm, stability and control tests must be carried out on each of the pre-established parameters to guarantee its optimal operation.

5.3. Sensitivity analysis with respect to various EV characteristics

In this section, we conduct two sensitivity analyses. Firstly, we examine the system's impact when charging EVs to different SOC levels in the EVCS. Secondly, we investigate the influence of the number of EVs connected to the EVCS. On days with high solar irradiance, the system accumulates an average of approximately 130 kWh of daily energy, considering the 30 kWp maximum power of the CCTI-B laboratory's PV system, as shown in Fig. 15(a). We evaluate the maximum SOC charging values for EVs: 20 %, 40 %, 60 %, 80 %, and 100 %. Results indicate that a fully charged EV battery reaches a maximum of about 20.4 kWh, representing 15.7 % of the PV generation capacity. Importantly, there is minimal difference between charging an EV to 20 % or 100 % SOC, due to the presence of VRFB, which redirect surplus energy to the grid after smoothing through the algorithm. This fixed data from the CCTI-B laboratory's equipment allows us to observe system variations and responses.

Fig. 15(b) displays the sensitivity analysis concerning the number of EVs connected to the EVCS. The system autonomously supports up to 5 EVs with an average photovoltaic energy generation of 100 kWh. On higher PV generation days, it can fully charge up to 6 EVs without requiring power grid. It is possible to see that the energy for each additional electric vehicle is approximately 20 kWh, which has a minimal impact on the system. In summary, the sensitivity analysis reveals insights into the system's performance in response to EV SOC levels and the number of connected EVs in various scenarios.

5.4. Economic evaluation

In this section, a cost estimation based on Table 1 is presented for integrated PV systems and sizing for SC and VRFB. Considering the power of the EVCS at 20 kWh, as analyzed earlier, it is possible to determine the cost and sizing for the PV system based on the number of EVs (N_{EV}), SOC_{EV}, and PV power (e.g., 6 kW generating 20 kWh) according to the energy it could deliver. The details are as follows in Eq. (16) [38].

$$C_{PV} = \frac{N_{EV} \times SOC_{EV} \times P_{GPV}}{100} \times 870 = 8.7 \times N_{EV} \times SOC_{EV} \times P_{GPV} \ [\text{USD/kW}] \tag{16}$$

where C_{PV} represent the total cost of PV, N_{EV} is the number of EV, SOC_{EV} is the SOC of EV, P_{GPV} is the peak PV power considers for full EV charge. Similarly, the cost and sizing estimation for VRFBs consider maintaining the SOC of VRFB at 25 % as the limit during the charging processes at any time of the day for the EV with power N_{EV} and charging time Δt_{EV}.

$$C_{VR} = \frac{0.75 \times N_{EV} \times SOC_{EV} \times P_{EV} \times \Delta t_{EV}}{100} \times 700 = 5.25 \times N_{EV} \times SOC_{EV} \times P_{GPV} \times \Delta t_{EV} \ [\text{USD/kWh}] \tag{17}$$

where C_{VR} represents the total cost of VRFB. Finally, an estimated value is established for the SC based on a 10 %/min reduction in PV fluctuations with a hybrid combination of VRFB and a nominal power of the PV system of 30 kW as follows.

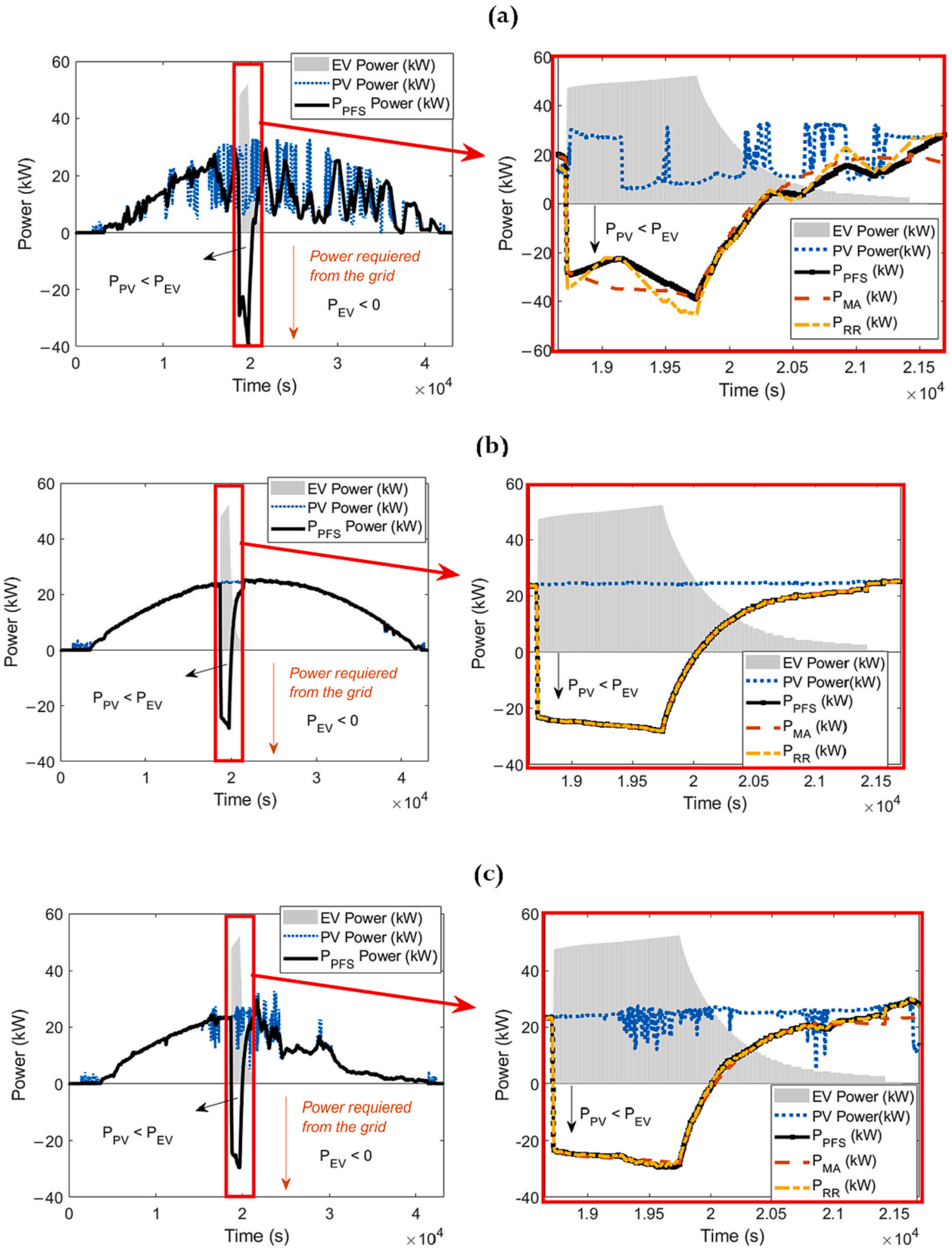

Fig. 13. Comparative analysis of MA, RR and PFS methods. (a) Little cloudiness. (b) Clear day. (c) Semi-clear day.

Table 5
Comparative criteria analysis of power smoothing methods.

Method	Fast response with high power density	Unlimited operating cycles	RR limitation10%	Energy supply for EVCS
PV + SC	X	X	Depends on PV nominal power	Requires significant SC capacity
PV + VRFB	–	X	X	X
PV + SC + VRFB	X	X	X	X

$$C_{SC} = \frac{N_{EV} \times P_{GPV} \times 0.4}{30} \times 27.5 \times 1000 = 360 \times N_{EV} \times P_{GPV} \text{ [USD/kWh]} \quad (18)$$

where C_{SC} is the total cost of SC. The results of Eqs. (16)–(18) are presented in Fig. 16(a) for different numbers of EVs at full charge 0–100 %, where the sizing of the VRFB and SC was characterized based on the experimental tests and on-site power. For example: The demand for 4 fully charged requires 80 kWh. Which is covered by a 21 kW PV system, 80 kWh VRFB and 0.3 kWh SC. Consequently, it would generate a total cost of approximately $C_{PV} + C_{VR} + C_{SC} =$ $ 71,520 for self-sustaining charging stations. On the other hand, Fig. 16(b) analyzes the cost implied by the system for 4 EVs with variable EV charging values. Considering the different charge probability of each EVs. That is, SOC_{EV} = 90 %, 80 %, 60 %, 50 %. It can be seen how the dimensioning for VRFB varies considerably, becoming competitive in prices with the PV system.

5.5. Future applications

Due to the gradual increase in EV within distribution electrical grids [41], a progressive replacement and adaptation of conventional gas stations to EVCS can be envisioned. As depicted in Fig. 17(a), this study proposes the integration of photovoltaic systems with SC and VRFB to mitigate power fluctuations and the impact of EV charging peaks on the electrical grid. This process, in the future, involves replacing areas designated for fuel storage with alternative means such as VRFB (see Fig. 17b), ensuring efficient use of space and environmental sustainability. In Fig. 17(c), the current map illustrates five charging stations in the city with potential expansion into specific zones. The CCTI-B,

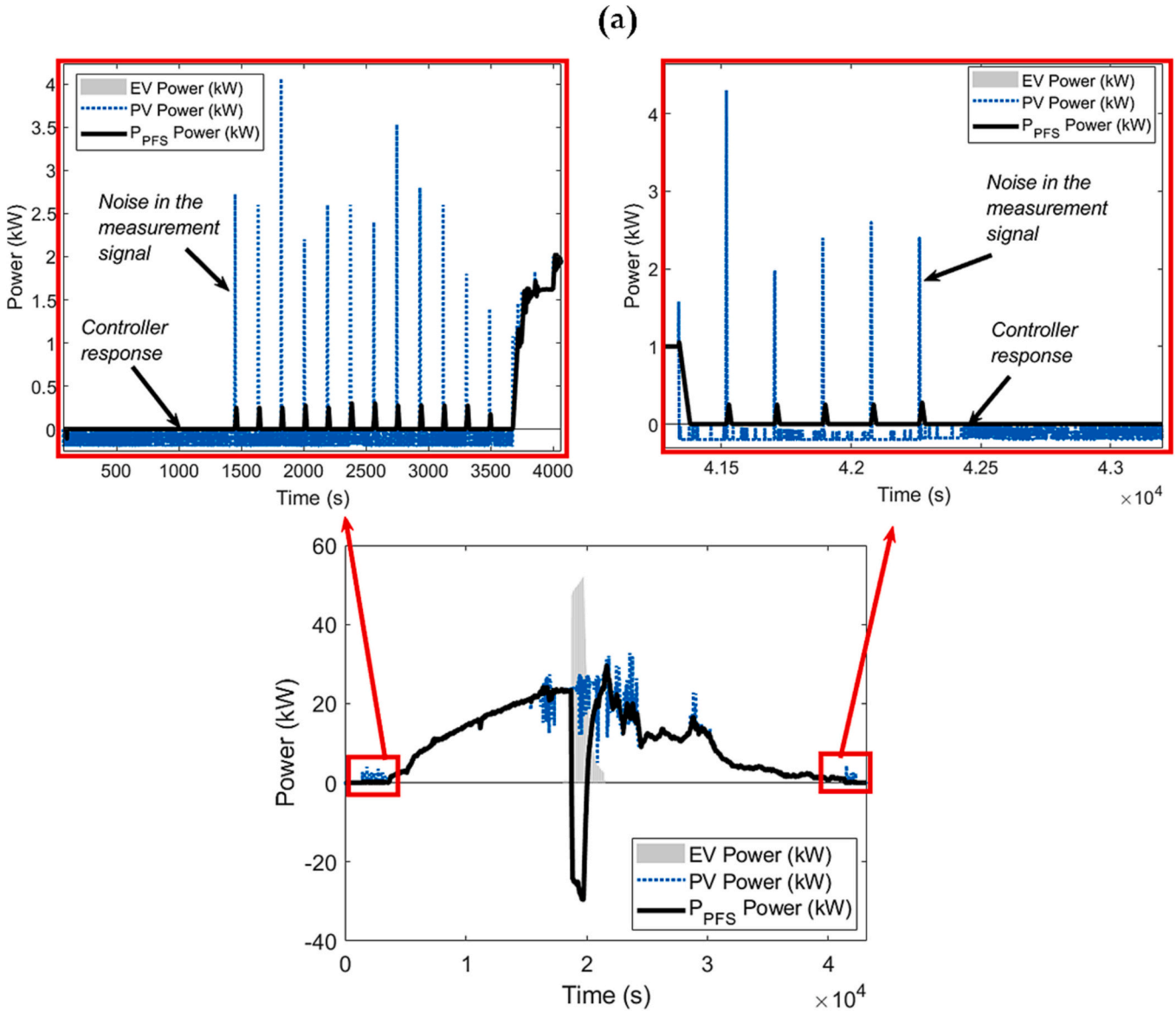

Fig. 14. Analysis of noise and disturbance signals: (a) Controller response to noise signals. (b) Controller response to disturbance signals.

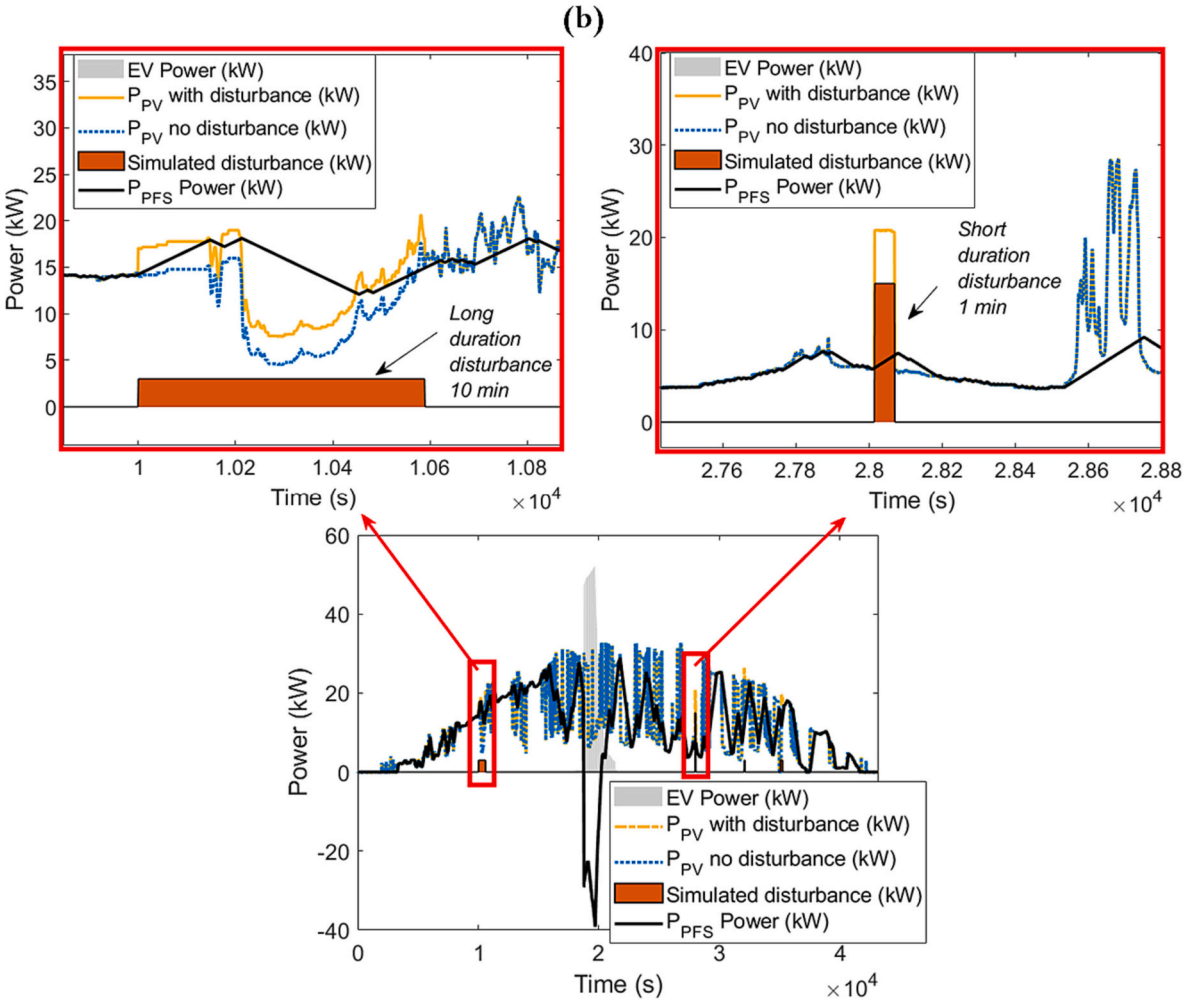

Fig. 14. (*continued*).

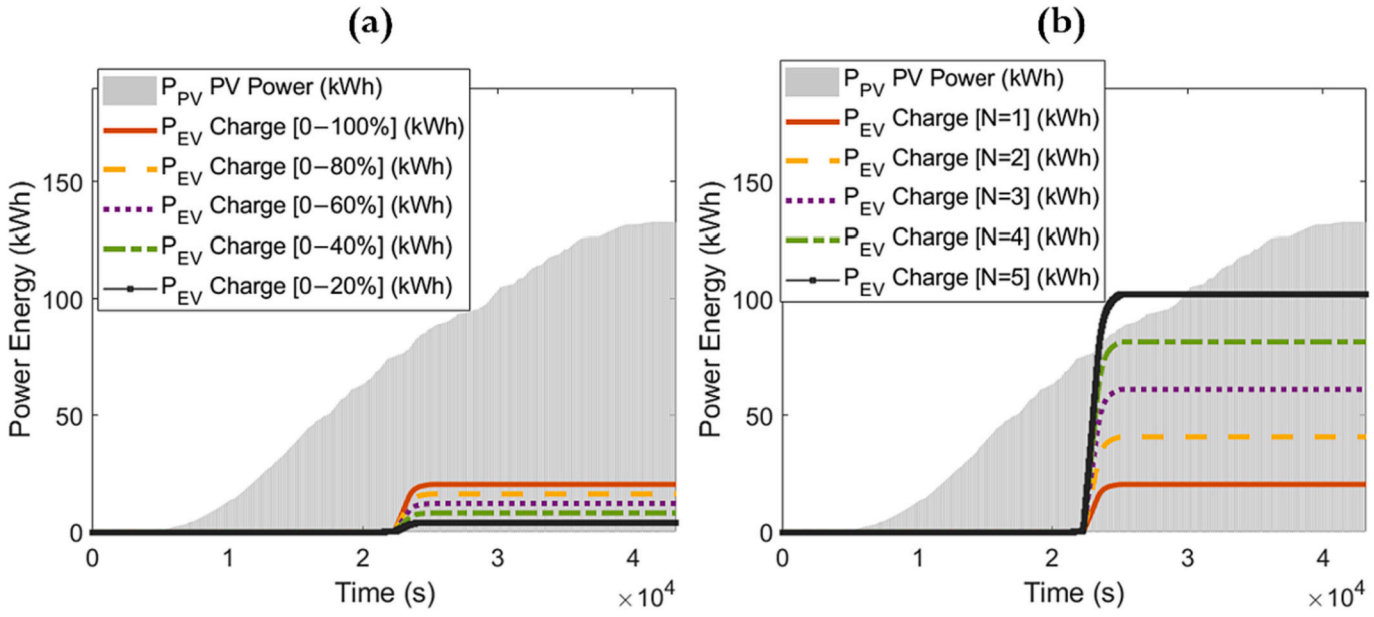

Fig. 15. Sensitivity analysis (a) EV SOC percentage. (b) Integration of EV number.

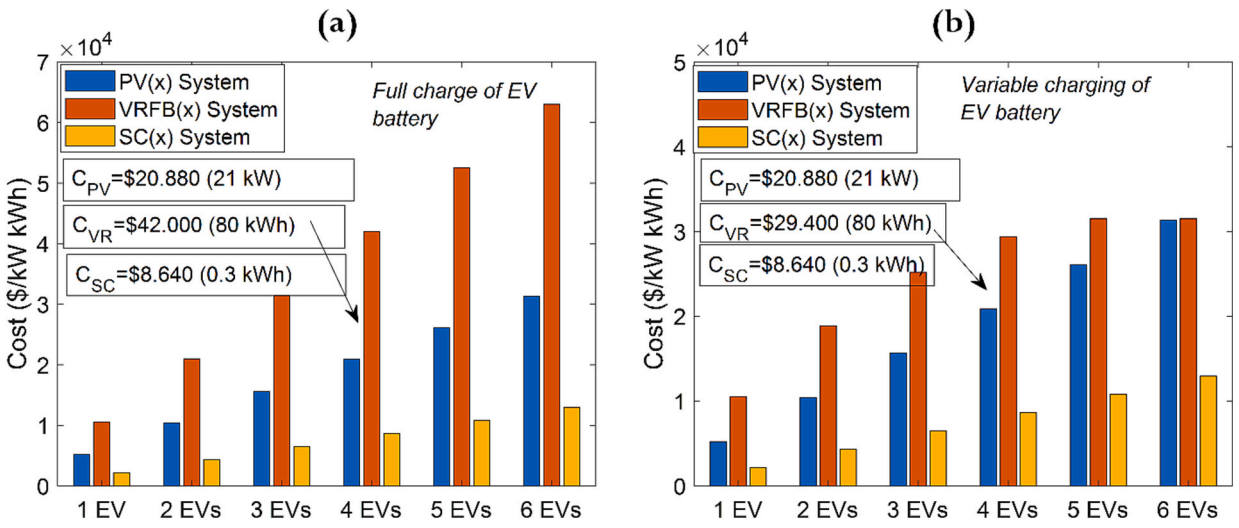

Fig. 16. Cost analysis for different number of EVs for self-sustaining charging stations. (a) Full charge of EV battery. (b) Variable charging of EV battery.

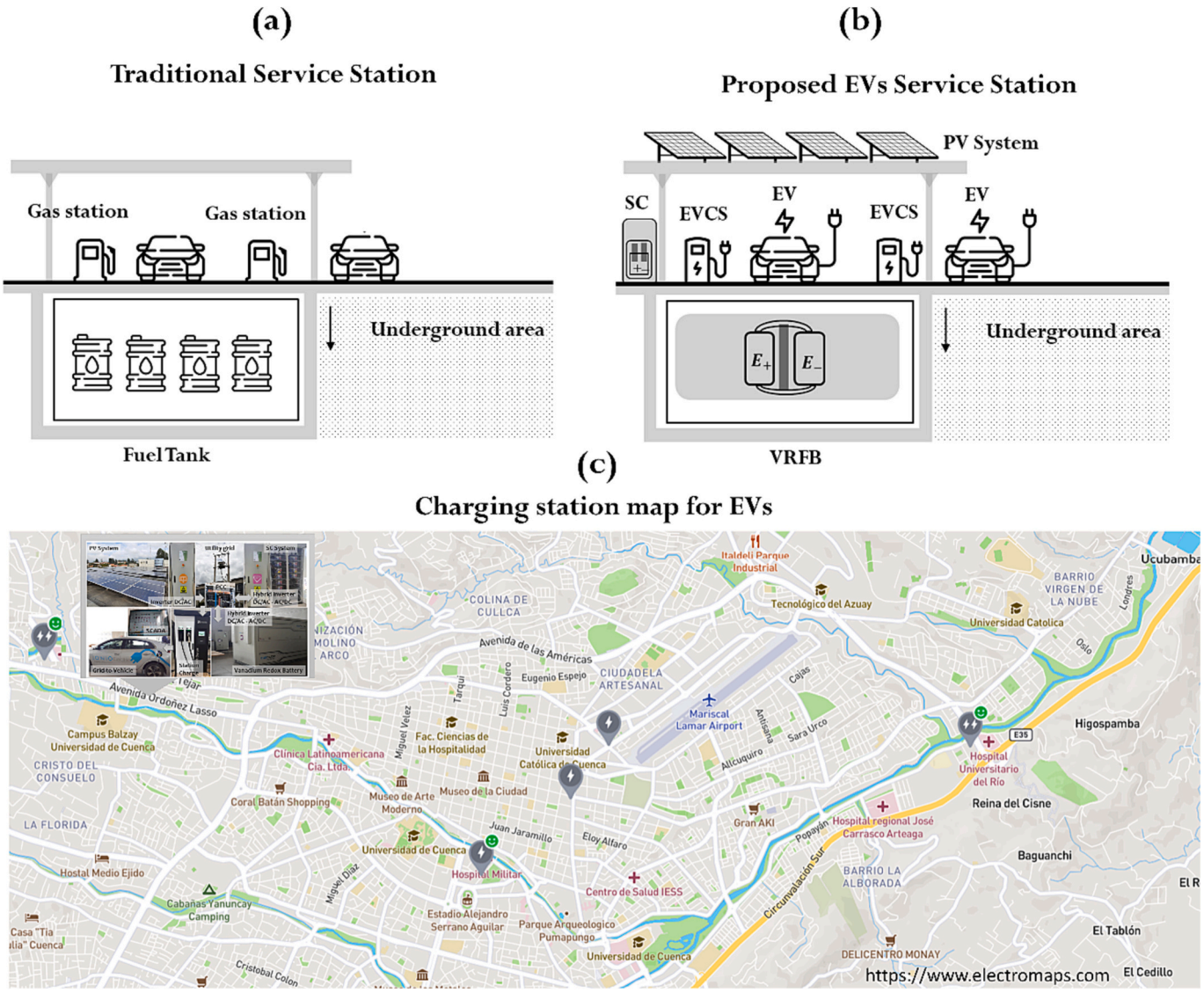

Fig. 17. Future fields of application of the case study: (a) Traditional service station. (b) Proposed EVs service station. (c) Charging station map for EVs.

considered as the baseline case study, will facilitate further investigations in this domain.

6. Conclusions

This paper introduces the predictive-flex smoother (PFS), a novel method designed to mitigate power fluctuations in grid-connected photovoltaic (PV) systems while optimizing energy management in electric vehicle charging stations (EVCS). The PFS method incorporates a hybrid energy storage system comprising supercapacitors (SC) and vanadium redox flow batteries (VRFB), utilizing prediction algorithms and machine learning techniques for precise power fluctuation forecasts. The study demonstrates the practical efficacy of the PFS method in real-time power smoothing, achieving minimal delays (approximately 500 ms). This results in enhanced stability by efficiently mitigating both PV and grid power fluctuations.

The integration of SC and VRFB in the PV + SC + VRFB configuration significantly improves power smoothing capabilities, meeting rapid response, unlimited operating cycles, and ramp rate limitation criteria. Comparative analyses under various weather conditions underscore the system's adaptability to diverse scenarios of PV energy generation and EV charging demand. The PV + SC + VRFB method optimizes surplus energy utilization while simultaneously reducing dependence on the grid. Performance comparisons with common methods, such as moving average (MA) and ramp rate (RR), highlight the superiority of the PFS method. It not only meets the 10 %/min ramp rate limit but also achieves superior power smoothing results, enhancing the overall performance and stability of the system.

Sensitivity analyses regarding EV state of charge (SOC) and the number of connected EVs underscore the system's flexibility in handling different charging scenarios. These analyses provide valuable insights for optimized performance and sizing, offering practical implications for real-world applications. The economic evaluation reveals that the PV + SC + VRFB system offers a cost-effective solution for self-sustaining charging stations. For example, charging 4 EVs at full load requires 80 kWh, covered by a 21 kW PV system, 80 kWh VRFB, and 0.3 kWh SC, resulting in a total cost of approximately $71,520 for self-sustaining charging stations.

CRediT authorship contribution statement

Darío Benavides: Software, Resources, Project administration, Methodology, Funding acquisition, Formal analysis. **Paul Arévalo:** Writing – original draft, Visualization, Validation, Supervision, Software, Resources, Project administration. **Edisson Villa-Ávila:** Software, Resources, Project administration, Methodology, Investigation, Funding acquisition, Formal analysis. **José A. Aguado:** Project administration, Methodology, Investigation, Funding acquisition, Formal analysis. **Francisco Jurado:** Visualization, Validation, Supervision, Software, Funding acquisition, Formal analysis, Data curation.

Declaration of competing interest

The authors declare that they have no known competing financial interests or personal relationships that could have appeared to influence the work reported in this paper.

Data availability

Data will be made available on request.

Acknowledgment

The first author is grateful for a Doctoral Training Program in the area of Engineering and Technical Sciences (UMA, Spain; UTI, UTM, UTN, Ecuador) of Asociación Universitaria Iberoamericana de Postgrado (AUIP).

The author (Paul Arévalo) thanks the Call for Grants for the Requalification of the Spanish University System for 2021–2023, Margarita Salas Grants for the training of young doctors awarded by the Ministry of Universities and financed by the European Union –Next Generation EU.

The authors thank Universidad de Cuenca for easing access to the facilities of the Microgrid Laboratory of the Centro Científico Tecnológico y de Investigación Balzay (CCTI-B), for allowing the use of its equipment, and for authorizing its staff the provision of technical support necessary to carry out the experiments described in this article.

The icons used in this document were developed by Freepik, monkik, Smashicons and Pixel perfect, from www.flaticon.com.

References

[1] K. Saberi-Beglar, K. Zare, H. Seyedi, M. Marzband, S. Nojavan, Risk-embedded scheduling of a CCHP integrated with electric vehicle parking lot in a residential energy hub considering flexible thermal and electrical loads, Appl. Energy 329 (2023) 120265, https://doi.org/10.1016/j.apenergy.2022.120265.

[2] Q. Chen, X. Li, Z. Zhang, C. Zhou, Z. Guo, Z. Liu, H. Zhang, Remote sensing of photovoltaic scenarios: techniques, applications and future directions, Appl Energy 333 (2023) 120579, https://doi.org/10.1016/J.APENERGY.2022.120579.

[3] H. Hou, M. Xue, Y. Xu, Z. Xiao, X. Deng, T. Xu, P. Liu, R. Cui, Multi-objective economic dispatch of a microgrid considering electric vehicle and transferable load, Appl. Energy 262 (2020) 114489, https://doi.org/10.1016/J.APENERGY.2020.114489.

[4] M. Jaszczur, Q. Hassan, An optimization and sizing of photovoltaic system with supercapacitor for improving self-consumption, Appl. Energy 279 (2020) 115776, https://doi.org/10.1016/J.APENERGY.2020.115776.

[5] S. Shivashankar, S. Mekhilef, H. Mokhlis, M. Karimi, Mitigating methods of power fluctuation of photovoltaic (PV) sources - a review, Renew. Sustain. Energy Rev. 59 (2016) 1170–1184, https://doi.org/10.1016/J.RSER.2016.01.059.

[6] C. Li, L. Zhang, Z. Ou, Q. Wang, D. Zhou, J. Ma, Robust model of electric vehicle charging station location considering renewable energy and storage equipment, Energy 238 (2022) 121713, https://doi.org/10.1016/J.ENERGY.2021.121713.

[7] B. Panda, A. Ghoshal, An ANN based switching network for optimally selected photovoltaic array with battery and supercapacitor to mitigate the effect of intermittent solar irradiance, Energy Sources, Part A 44 (2022) 5784–5811, https://doi.org/10.1080/15567036.2022.2088897.

[8] S. Sraidi, M. Maaroufi, Dynamic wireless charging of electric vehicles: supercapacitor integration at the service of energy management optimization, Electrica 23 (2023) 449–457, https://doi.org/10.5152/ELECTRICA.2023.22014.

[9] H. Zhang, Y. Cheng, D.G. Lek, T. Liu, F. Lin, W. Luo, S. Huang, M. Gao, X. Wang, Y. Zhi, et al., Membrane-free redox flow cell based on thermally regenerative electrochemical cycle for concurrent electricity storage, cooling and waste heat harnessing of perovskite solar cells, J. Power Sources 548 (2022) 232081, https://doi.org/10.1016/J.JPOWSOUR.2022.232081.

[10] S. Akagi, S. Yoshizawa, M. Ito, Y. Fujimoto, T. Miyazaki, Y. Hayashi, K. Tawa, T. Hisada, T. Yano, Multipurpose control and planning method for battery energy storage systems in distribution network with photovoltaic plant, International Journal of Electrical Power and Energy Systems 116 (2020) 105485, https://doi.org/10.1016/J.IJEPES.2019.105485.

[11] C. Jamroen, E. Usaratniwart, S. Sirisukprasert, PV power smoothing strategy based on HELES using energy storage system application: a simulation analysis in microgrids, IET Renewable Power Generation 13 (2019) 2298–2308, https://doi.org/10.1049/IET-RPG.2018.6165.

[12] D. Benavides, P. Arévalo, J.A. Aguado, F. Jurado, Experimental validation of a novel power smoothing method for on-grid photovoltaic systems using supercapacitors, International Journal of Electrical Power and Energy Systems 149 (2023) 109050, https://doi.org/10.1016/J.IJEPES.2023.109050.

[13] X. Han, X. Liu, H. Wang, Dual-regulating feedback optimization control of distributed energy storage system in power smoothing scenariox based on KF-MPC, IEEE Access 8 (2020) 172601–172609, https://doi.org/10.1109/ACCESS.2020.3025334.

[14] M. Raoofat, M. Saad, S. Lefebvre, D. Asber, H. Mehrjedri, L. Lenoir, Wind power smoothing using demand response of electric vehicles, Int. J. Electr. Power Energy Syst. 99 (2018) 164–174, https://doi.org/10.1016/J.IJEPES.2017.12.017.

[15] Y. Belkhier, A. Oubelaid, Novel design and adaptive coordinated energy management of hybrid fuel-cells/tidal/wind/PV array energy systems with battery storage for microgrids, Energy Storage 6 (2024) e556, https://doi.org/10.1002/EST2.556.

[16] M. Singh, P. Kumar, I. Kar, A multi charging station for electric vehicles and its utilization for load management and the grid support, IEEE Trans Smart Grid 4 (2013) 1026–1037, https://doi.org/10.1109/TSG.2013.2238562.

[17] M. Jannati, S.H. Hosseinian, B. Vahidi, G. Li, Jie a significant reduction in the costs of battery energy storage systems by use of smart parking lots in the power fluctuation smoothing process of the wind farms, Renew. Energy 87 (2016) 1–14, https://doi.org/10.1016/J.RENENE.2015.09.054.

[18] B. Cortés-Caicedo, F. Molina-Martin, L.F. Grisales-Noreña, O.D. Montoya, J. C. Hernández, Optimal design of PV systems in electrical distribution networks by minimizing the annual equivalent operative costs through the discrete-continuous

vortex search algorithm, Sensors 22 (2022) 851, https://doi.org/10.3390/S22030851.
[19] J. Zhang, L. Hou, X. Diao, X. Yang, P. Tang, X. Cao, Power allocation method of battery energy storage system considering state balance in smoothing photovoltaic power fluctuations, Front Energy Res 10 (2022) 965812, https://doi.org/10.3389/FENRG.2022.965812.
[20] K. Bachiri, A. Yahyaouy, H. Gualous, M. Malek, Y. Bennani, P. Makany, N. Rogovschi, Multi-agent DDPG based electric vehicles charging station recommendation, Energies 16 (2023) 6067, https://doi.org/10.3390/EN16166067.
[21] S. Hossain, M. Rokonuzzaman, K.S. Rahman, A.K.M.A. Habib, W.S. Tan, M. Mahmud, S. Chowdhury, S. Channumsin, Grid-vehicle-grid (G2V2G) efficient power transmission: an overview of concept, operations, benefits, concerns, and future challenges, Sustainability (Switzerland) 15 (2023) 5782, https://doi.org/10.3390/SU15075782.
[22] M.T. Hussain, D.N. Bin Sulaiman, M.S. Hussain, M. Jabir, Optimal management strategies to solve issues of grid having electric vehicles (EV): a review, J Energy Storage 33 (2021) 102114, https://doi.org/10.1016/J.EST.2020.102114.
[23] C.T. Ma, System planning of grid-connected electric vehicle charging stations and key technologies: a review, Energies (Basel) 12 (2019) 4201, https://doi.org/10.3390/EN12214201.
[24] Á. Cunha, F.P. Brito, J. Martins, N. Rodrigues, V. Monteiro, J.L. Afonso, P. Ferreira, Assessment of the use of vanadium redox flow batteries for energy storage and fast charging of electric vehicles in gas stations, Energy 115 (2016) 1478–1494, https://doi.org/10.1016/J.ENERGY.2016.02.118.
[25] Y.S. Lee, H.J. Yoon, J.W. Shim, Collective power smoothing functionality of renewable energy sources with energy storage system, Journal of Electrical Engineering and Technology 1 (2023) 1–11, https://doi.org/10.1007/S42835-023-01727-1.
[26] A.I. Nousdilis, G.C. Kryonidis, T.A. Papadopoulos, Comparative evaluation of solar power smoothing techniques considering battery degradation, IEEE J Photovolt 13 (2023) 951–957, https://doi.org/10.1109/JPHOTOV.2023.3308259.
[27] A.A. Abdalla, M.S. El Moursi, T.H. El-Fouly, K.H. Al Hosani, A novel adaptive power smoothing approach for PV power plant with hybrid energy storage system, IEEE Trans Sustain Energy 14 (2023) 1457–1473, https://doi.org/10.1109/TSTE.2023.3236634.
[28] L. Wang, W.J.Y. Ke, R.X. Wu, M. Tripathy, H. Mokhlis, K.H. Chua, A.V. Prokhorov, T.H. Nguyen, M.M. Farid, A. Subiantoro, et al., Stability evaluation of a grid-tied hybrid wind/PV farm joined with a hybrid energy-storage system, Sustainable Environment Research 33 (2023) 00181, https://doi.org/10.1186/S42834-023-00181-Y.
[29] Q. Chai, C. Zhang, Z. Tong, S. Lu, W. Chen, Z.Y. Dong, PV inverter reliability constrained volt/var control with power smoothing via a convex-concave programming method, IEEE Trans. Industr. Inform. 19 (2023) 109–120, https://doi.org/10.1109/TII.2022.3165643.
[30] R.C. de Barros, D. Gonçalves, A.F. Cupertino, V.F. Mendes, W. do Couto Boaventura, H.A. Pereira, Wear-out analysis of a BESS converter under peak shaving and harmonic current compensation, Microelectron. Reliab. 150 (2023) 115099, https://doi.org/10.1016/J.MICROREL.2023.115099.
[31] M.K. Behera, L.C. Saikia, A novel resilient control of grid-integrated solar PV-hybrid energy storage microgrid for power smoothing and pulse power load accommodation, IEEE Trans. Power Electron. 38 (2023) 3965–3980, https://doi.org/10.1109/TPEL.2022.3217144.
[32] E. Villa-Ávila, P. Arévalo, D. Ochoa-Correa, V. Iñiguez-Morán, F. Jurado, Innovative power smoothing technique for enhancing renewable integration in insular power systems using electric vehicle charging stations, Applied Sciences 14 (2023) 375, https://doi.org/10.3390/APP14010375.
[33] M. Wang, L. Ge, C. Dong, Q. Xiao, H. An, Y. Mu, Smoothing control of wind power fluctuations with battery energy storage system of electric vehicles, International Transactions on Electrical Energy Systems 31 (2021) e12606, https://doi.org/10.1002/2050-7038.12606.
[34] T. Qian, C. Shao, X. Li, X. Wang, Z. Chen, M. Shahidehpour, Multi-agent deep reinforcement learning method for EV charging station game, IEEE Trans. Power Syst. 37 (2022) 1682–1694, https://doi.org/10.1109/TPWRS.2021.3111014.
[35] H.J. Feng, L.C. Xi, Y.Z. Jun, Y.X. Ling, H. Jun, Review of electric vehicle charging demand forecasting based on multi-source data, in: Proceedings of the iSPEC 2020 - Proceedings: IEEE Sustainable Power and Energy Conference: Energy Transition and Energy Internet, Institute of Electrical and Electronics Engineers Inc., November 23 2020, pp. 139–146.
[36] G. Wang, M. Ciobotaru, V.G. Agelidis, Power smoothing of large solar PV plant using hybrid energy storage, IEEE Trans Sustain Energy 5 (2014) 834–842, https://doi.org/10.1109/TSTE.2014.2305433.
[37] G. Wang, M. Ciobotaru, V.G. Agelidis, Power management for improved dispatch of utility-scale PV plants, IEEE Trans. Power Syst. 31 (2016) 2297–2306, https://doi.org/10.1109/TPWRS.2015.2459065.
[38] X. Liu, Z. Bie, Optimal allocation planning for public EV charging station considering AC and DC integrated chargers, Energy Procedia 159 (2019) 382–387, https://doi.org/10.1016/J.EGYPRO.2018.12.072.
[39] IRENA, Renewable Power Generation Costs in 2021; Abu Dhabi 2022, 2021.
[40] The CellCube system - Cellcube, Available online: https://www.cellcube.com/the-cellcube-system/ (accessed on 6 January 2024).
[41] S. Gao, J. Wu, B. Xu, Controllability evaluation of EV charging infrastructure transformed from gas stations in distribution networks with renewables, Energies 12 (2019) 1577, https://doi.org/10.3390/EN12081577.